Engineering Applications of Artificial Intelligence 151 (2025) 110723

Contents lists available at ScienceDirect

Engineering Applications of Artificial Intelligence

journal homepage: www.elsevier.com/locate/engappai

Advanced multi-layer deep learning model for accurate estimation of heat transfer and flow designing parameters across diverse dataset configurations

Ali A.H. Karah Bash [a], Ahmad Aboul Khail [b,c,*,1]

[a] Department of Electrical and Electronic Engineering, Faculty of Engineering, Hasan Kalyoncu University, Şahinbey, Postal code: 27110, Gaziantep, Türkiye
[b] Department of Mechanical Engineering, Faculty of Engineering, Hasan Kalyoncu University, Şahinbey, Postal code: 27110, Gaziantep, Türkiye
[c] Department of Nuclear Engineering, Faculty of Mechanical Engineering, Aleppo University, Aleppo, Syria

ARTICLE INFO

Keywords:
Advanced plate heat exchanger
Nusselt number
Friction factor
Performance parameter
Classical deep learning models
Hybrid deep learning model

ABSTRACT

This study introduces a hybrid deep learning (DL) model for accurately predicting key parameters of Advanced plate heat exchanger (APHE) performance, including the Nusselt number (*Nu*), friction factor (f), and thermal performance parameter (P). The hybrid deep learning (DL) model integrates multiple deep learning (DL) models—Feedforward Neural Network (FNN), Cascade Forward Neural Network (CFNN), and Fitting Network (FN)—in a multi-layered design to optimize predictive accuracy. Evaluations were conducted using five diverse datasets, each divided into three scenarios targeting *Nu*, f, and P, respectively, thereby capturing a broad range of thermal system behaviors. The experimental analysis reveals that the proposed hybrid DL model delivers outstanding predictive accuracy, as reflected in the following results. For *Nu* prediction, the Root Mean Square Error (RMSE) of the top models in the second layer ranged from 0.0003 to 0.00305 across various datasets. In the case of predicting f, the RMSE spanned from 0.0002 to 0.0041, while for predicting P, it varied between 0.0001 and 0.0004. Notably, the third layer retained CFNN as the most effective architecture, achieving remarkably low RMSE values of 8.1×10^{-6}, 4.8×10^{-6}, and 4.86×10^{-6} for *Nu*, f, and P, respectively. Mean Absolute Error (MAE) and Nash-Sutcliffe Efficiency (NSE) metrics further validated the model's robustness, consistently yielding NSE scores near 0.9999. These models effectively minimized errors, particularly in high-variability regions. In the third layer, the hybrid DL framework selected CFNN as the optimal DL model for final predictions across all scenarios. This refinement achieved near-perfect accuracy, with Coefficient of Determination (R^2) values surpassing 0.9999 and RMSE values reduced to less than 0.00003, showcasing exceptional generalization and reliability. The hybrid DL model consistently outperformed standalone DL models by combining their strengths and leveraging a hierarchical architecture. These results highlight the potential of hybrid DL approaches in addressing complex regression tasks and advancing predictive modeling in engineering applications. This study provides a significant contribution to optimizing heat exchanger performance and demonstrates the utility of hybrid DL models in real-world thermal system challenges.

Nomenclature

Re	Reynolds number	*Nu*	Nusselt number
f	Friction factor	**P**	Pressure drop
a_mm	The radius of the ellipse along the major axis	**b_mm**	The radius of the ellipse along the minor axis

(*continued on next column*)

(*continued*)

Re	Reynolds number	*Nu*	Nusselt number
PHE	Plate Heat Exchanger	**APHE**	Advanced Plate Heat Exchanger
MHEs	Micro Heat Exchangers	**FNN**	Feedforward Neural Network

(*continued on next page*)

* Corresponding author. Department of Mechanical Engineering, Faculty of Engineering, Hasan Kalyoncu University, Şahinbey, Postal code: 27110, Gaziantep, Türkiye.
E-mail addresses: ali.karabash@hku.edu.tr, ali_karabash2016@yahoo.com (A.A.H. Karah Bash), khailnuc@gmail.com, ahmed.sadik@hku.edu.tr (A.A. Khail).
[1] Because the author holds dual citizenship, his name can be presented in two formats: Ahmad Aboul Khail or Ahmed Sadık.

https://doi.org/10.1016/j.engappai.2025.110723
Received 3 January 2025; Received in revised form 1 March 2025; Accepted 27 March 2025
Available online 1 April 2025

(*continued*)

Re	Reynolds number	*Nu*	Nusselt number
CFNN	Cascade Forward Neural Network	**FN**	Fit Neural Network
RBFNN	Radial Basis Function Neural Network	**ReLU**	Rectified Linear Unit, an activation function
Tanh	Hyperbolic tangent activation function	**Learning Rate**	Step size during model training optimization
Epochs	Number of complete passes through the training dataset	**Adam**	Adaptive Moment Estimation optimization algorithm
SGD	Stochastic Gradient Descent optimization method	**RMSProp**	Root Mean Square Propagation Optimizer
LM	Levenberg-Marquardt optimization algorithm	**BR**	Bayesian Regularization for reducing model overfitting
RMSE	Root Mean Square Error	**MAE**	Mean Absolute Error
R^2	Coefficient of Determination	**SI**	Scatter Index
NSE	Nash–Sutcliffe Efficiency	**ML**	Machine Learning
DL	Deep Learning	**MHEs**	Multi Heat Exchangers
BT	Boosting Trees	**SVR**	Support Vector Regression
GPR	Gaussian Process Regression	**LR**	Linear Regression
DT	Decision Tree	**HEs**	Heat Exchangers
PCHE	Printed Circuit Heat Exchanger	**CFD**	Computational Fluid Dynamics
BRF	Bootstrap Random Forest	**MLR**	Multiple Linear Regression
SVM	Support Vector Machine	**ANN**	Artificial Neural Network
CNN	Convolutional Neural Network	**GBM**	Gradient Boosting Machine
GA	Genetic Algorithm	**MLFNN**	Multilayer Feedforward Neural Network
J	Colburn factor	**RF**	Random Forest
LSTM	Long Short-Term Memory	**BO**	Bayesian Optimizations
NANN	Nonlinear Autoregressive Neural Network	**IQR**	Inter-Quartile Range

1. Introduction

Heat exchangers play a pivotal role in various industrial applications, including power generation, chemical processing, and refrigeration systems. Their efficiency and performance directly influence energy consumption and operational costs. To optimize their functionality, predicting critical parameters such as the Nusselt number (*Nu*), friction factor (f), and thermal performance parameter (P) is essential. These parameters are indicative of heat transfer rates, flow resistance, and overall thermal efficiency, making their accurate estimation vital for system design and operation. The ML and DL algorithms like NANN, cross-validation and BO models, and GPR (Jin, 2024; Jin et al., 2024a, 2024b, 2024c) are used as effective tools in the designing and the regression. These algorithms can also enable high-accuracy analysis of large and complex operational data, helping to identify patterns and relationships between key operational parameters such as heat transfer coefficient, friction factor (f), and pressure drop (p). They also contribute to performance prediction and design optimization by simulating multiple scenarios at lower costs and time compared to traditional methods. This makes them an ideal choice for supporting decision-making and achieving sustainable improvements in energy efficiency and thermal performance.

ML techniques were utilized by Godasiaei and Chamkha, 2024b to investigate how solid formation fouling affects the performance of MHEs. Advanced ML algorithms were also employed to uncover the mechanisms of thermal transfer processes and predict their influencing factors in molten salt heat exchangers (Godasiaei and Chamkha, 2024a). Several ML approaches, such as BT, SVR, GPR, DT, and LR, have been applied alongside process and performance factors to predict the fouling coefficient in HEs (Hosseini et al., 2022). Saeed et al. explored the improvement in PCHE performance within a Reynolds number range of 2500–60,000 through the application of ML techniques and CFD analysis (Saeed et al., 2022). The BRF method is utilized to evaluate the efficiency of a double-tube heat exchanger by integrating key variables, including *Nu* and f (Sammil et al., 2024). Mudhsh et al. (2023) modeled the flow characteristics using a Fire Hawk optimizer in combination with ML techniques and compared the results to those obtained from alternative methods. A novel prediction method was implemented, leveraging production costs and heat efficiency as assessment factors, with a multi-criteria approach integrating ANN for the optimal design of the PHE (Jilak et al., 2017). Uguz utilized ML methods, including ANN, MLR, and SVM, to predict the outlet temperature of the working fluid and assess the performance of a PHE fabricated using MAM technology, comparing the outcomes from each approach (Uguz et al., 2022a). Amalfi proposed a method that considers the exchanger's geometry and thermo-hydraulic conditions to predict the heat transfer coefficient and friction-induced pressure drop during flow boiling (Amalfi et al., 2021). A novel prediction approach was adopted, using production costs and heat efficiency as key evaluation factors, while a multi-criteria framework integrated ANN for optimizing the PHE configuration (Jilak et al., 2020). Wang et al. (2021) investigated the influence of air bubbles in water on flow dynamics through the application of CNN. The GBM model was utilized to predict the pressure drop, considering plate dimensions, operating conditions, and fluid properties (Longo et al., 2020). Khan et al. employed a gray-box model to forecast the optimal operating parameters for the working fluid flows (Khan et al., 2023). A combination of GA and MLFNN methods was applied to predict pressure loss, total cost, overall weight, and the f and j factors. (Peng et al., 2008, 2009).

Recent advancements in artificial intelligence, particularly deep learning (DL) (Hong et al., 2023, 2024; Wu et al., 2021), have opened new pathways for tackling complex regression tasks in engineering domains. Unlike traditional modeling approaches, DL models excel in capturing intricate, non-linear relationships within data, offering superior predictive capabilities. (Shah et al., 2024; Guo et al., 2024). However, the standalone application of DL models often encounters challenges, including overfitting and reduced generalization when applied to diverse datasets with varying thermal conditions.

To address these limitations, hybrid deep learning (DL) frameworks have emerged as a promising alternative. These frameworks integrate multiple DL architectures, leveraging their unique strengths to improve prediction accuracy and robustness (Uguz et al., 2022b). This study introduces a hybrid DL model designed to predict the targets with high accuracy. The proposed model employs Feedforward Neural Networks (FNN), Cascade Forward Neural Networks (CFNN), and Fitting Networks (FN) in a multi-layered structure, combining their advantages to achieve superior performance.

Accurate prediction of thermal performance parameters in heat exchangers has long been a subject of extensive research. Early studies predominantly relied on empirical correlations and computational fluid dynamics (CFD) simulations to estimate parameters such as *Nu* and f (Kakac et al., 2012). While these approaches provided valuable insights, their dependency on predefined assumptions often limited their applicability to complex and variable operational conditions. The advent of ML techniques marked a significant shift in this domain. Regression models, including SVM and RF, demonstrated improved predictive accuracy compared to traditional methods (Aboul Khail et al., 2024). However, these methods struggled with high-dimensional data and non-linear relationships, necessitating more advanced approaches.

DL has recently emerged as a transformative tool for predictive modeling in thermal systems. DL models such as FNN and LSTM networks have been successfully applied to predict heat transfer coefficients and pressure drops in heat exchangers (Wang et al., 2025). Despite their success, standalone DL models are often prone to overfitting and may fail to generalize across diverse datasets. To overcome these challenges, hybrid DL frameworks have gained attention in recent years. For instance, Wang et al. (2025) proposed a hybrid model integrating CNN

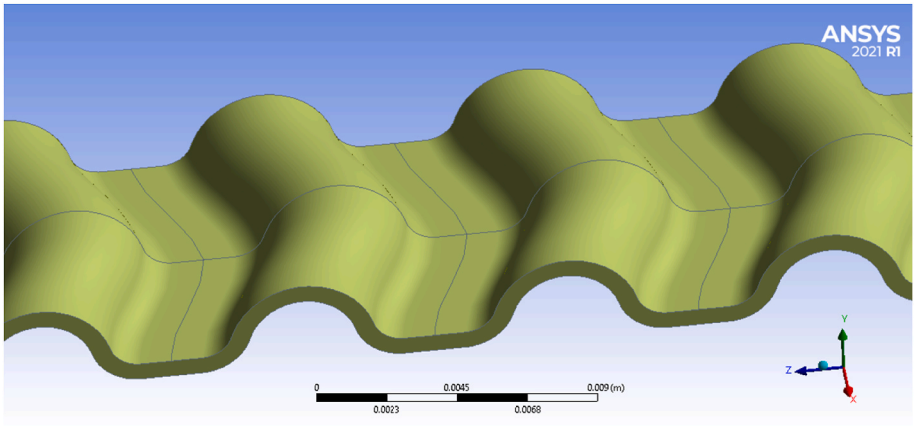

Fig. 1. Novel plate geometry.

and LSTM for temperature prediction in heat exchangers, achieving notable improvements in accuracy and robustness. Similarly, Ebbs-Picken et al. (Ebbs-Picken, 2024) developed a deep encoder-decoder hierarchical CNN for thermal efficiency prediction, demonstrating superior performance compared to standalone models. Most of the literature surveyed on engineering applications, especially in heat exchangers, tended to forecast exchanger design and operating characteristics using traditional hybrid models and classical algorithms. Conversely, the current study seeks to fill the gap left by previous research by employing a sophisticated hybrid DL model that improves the predictive power of the fundamental flow features in APHE. The current study integrates FNN, CFNN, and FN in a multi-layered framework. Unlike previous studies, this model is specifically designed to predict *Nu*, f, and P across diverse datasets, addressing the limitations of standalone models and achieving state-of-the-art performance. By incorporating five distinct datasets and three unique scenarios for each, the study ensures a comprehensive evaluation of the hybrid DL framework, setting a new benchmark for predictive modeling in thermal systems. The study evaluates the hybrid DL model using five diverse datasets, each representing different thermal system behaviors under three scenarios targeting *Nu*, f, and P. The results demonstrate the model's exceptional ability to generalize across varying conditions, achieving near-perfect accuracy and minimal error rates. This paper highlights the potential of hybrid DL models in advancing predictive modeling for heat exchanger optimization, thereby contributing to improved energy efficiency and reduced operational costs in industrial systems.

The primary contributions of this research are outlined as follows:

1) **Innovative Layered Hybrid Architecture:** The study proposes an innovative DL framework that integrates FNN, CFNN, and FN into a multi-layered design. This architecture harnesses the complementary strengths of these models, ensuring enhanced predictive accuracy and robustness.
2) **Comprehensive Evaluation Across Diverse Datasets:** The study evaluates the proposed hybrid DL model using five distinct datasets, each categorized into three scenarios targeting key performance parameters: Nusselt number (*Nu*), friction factor (f), and thermal performance parameter (P). This diverse dataset configuration captures a wide range of thermal system behaviors, ensuring the model's generalization and scalability.
3) **Dynamic Feature Refinement:** The novel methodology, which allows for the introduction of enhanced feature sets between multiple model layers, helps the model discover complex patterns, thus providing better predictive performance than traditional DL methods.
4) **Layer-wise model Optimization:** The study introduces a novel approach to model selection and refinement through its multi-layered structure. In the second layer, CFNN and FN were identified as the best-performing models across most datasets and scenarios. In the third layer, CFNN was selected as the optimal model, achieving the highest accuracy and reliability for final predictions.
5) **Scenario-Based Evaluation:** The extensive evaluation across five distinct datasets with three scenarios provides a robust analysis, showcasing the model's adaptability to varying data distributions.
6) **Efficient Model Selection:** By strategically reducing the number of models at each layer, the approach balances computational efficiency with prediction accuracy, setting it apart from traditional monolithic architectures.
7) **Generalizability and Scalability:** The framework is designed to be adaptable to other datasets, making it a scalable solution for future regression challenges beyond the current problem domain.
8) **Application to Complex Engineering Tasks:** The successful application of the proposed model to predict critical outputs (*Nu*, f, P) demonstrates its potential as a powerful tool for solving complex regression problems in engineering and industrial domains.

In summary, this study not only introduces a cutting-edge hybrid DL model but also establishes its superiority through rigorous evaluation, setting a precedent for the application of AI in solving complex engineering challenges. These contributions position the study as a valuable resource for both academic research and industrial applications.

2. Methodology

2.1. Mathematical modeling

2.1.1. Description of the innovative plate geometry

A new innovative plate for PHE was designed using basic units with curvature based on the "hyperbolic tangent function" where the cross-sectional shape of the basic unit is semi-elliptical (see Fig. 1) (Aboul Khail and Erişen, 2021). This design aims to enhance fluid mixing and increase transverse turbulence, resulting in improved heat transfer between the fluids inside the exchanger. The design is distinguished by its ability to promote mixing and disturb the boundary layer without significantly increasing the friction factor f. Comparisons showed that the Nusselt number *Nu* for this design is higher than other designs, including conventional Chevron plates and newer designs, positively impacting the exchanger's overall performance (Aboul Khail et al., 2022). The superiority of this design lies in the innovative geometry of the basic units, which enhances thermal mixing efficiency and improves performance based on the criterion $\mathbf{Nu/f^{1/3}}$, outperforming other designs.

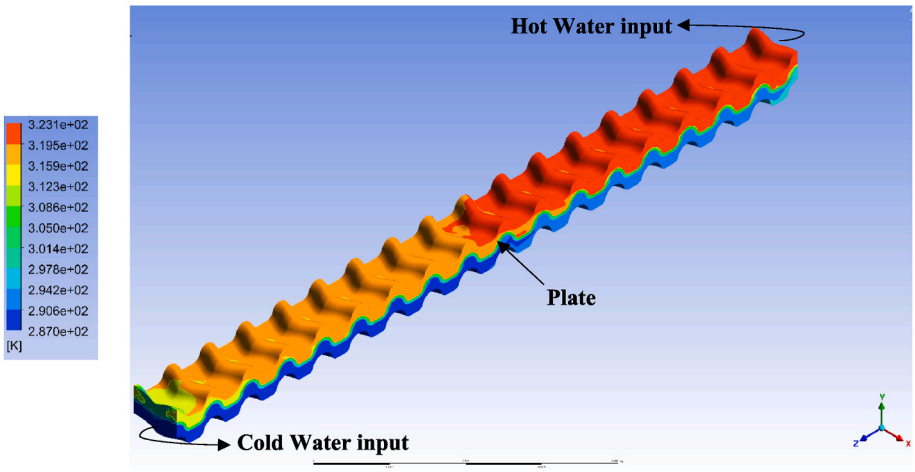

Fig. 2. Temperatures map of the channel.

2.1.2. The governing mathematical model for numerical modeling

The flow and analysis of thermal and hydrodynamic properties of the proposed model were described using governing equations based on the fundamental principles of thermodynamics and fluid mechanics. These equations include the continuity equation, which represents the law of mass conservation, ensuring that the mass flow rate entering and exiting any point remains constant. The Navier-Stokes equations describe the momentum balance on a unit volume of fluid, incorporating pressure, viscous, and gravitational forces. The energy equation is used to conserve energy, accounting for heat transfer by conduction and convection. To ensure the accuracy and precision of the results, a set of assumptions was adopted to simplify the calculations. First, the flow was assumed to be in a steady state, neglecting any temporal changes in flow and temperature. Fluid properties, such as density and viscosity, were considered constant and invariant over time and space. Accordingly, the numerical modeling equations (continuity, Navier-Stokes, and energy) can be formulated as follows:

$$\frac{\partial u_x}{\partial x}+\frac{\partial u_y}{\partial y}+\frac{\partial u_z}{\partial z}=0$$

$$u_x\frac{\partial u_i}{\partial x}+u_y\frac{\partial u_i}{\partial y}+u_z\frac{\partial u_i}{\partial z}=-\frac{1}{\rho}\frac{\partial p}{\partial x_i}+\nu\left[\frac{\partial^2 u_i}{\partial x^2}+\frac{\partial^2 u_i}{\partial y^2}+\frac{\partial^2 u_i}{\partial z^2}\right]\quad ;\ i=z,y,x$$

$$u_x\frac{\partial T}{\partial x}+u_y\frac{\partial T}{\partial y}+u_z\frac{\partial T}{\partial z}=\alpha\left[\frac{\partial^2 T}{\partial x^2}+\frac{\partial^2 T}{\partial y^2}+\frac{\partial^2 T}{\partial z^2}\right]$$

Due to the geometric characteristics of the plate design, the flow was assumed to be turbulent (Re > 400) (Aboul Khail and Erişen, 2023) as described under the "turbulent flow" conditions in PHEs. In the study, the **Shear Stress Transport (SST) k- ω** model was adopted as the **turbulence model** to analyze the flow characteristics. This model combines the advantages of the **k−ω** model near walls, where boundary layer effects are significant, and the **k−ε** model in regions away from the walls. This makes it suitable for analyzing turbulent flows in complex geometries like the new plate design. The equations used to model the **SST k- ω** are as follows:

Turbulent Kinetic Energy Equation k:

$$\frac{\partial(\rho u_i k)}{\partial x_i}=P_k-\beta^*\rho k\omega+\frac{\partial}{\partial x_i}\left[(\mu+\sigma_k\mu_t)\frac{\partial k}{\partial x_i}\right]$$

$$\frac{\partial(\rho u_i \omega)}{\partial x_i}=\alpha\frac{\omega}{k}P_k-\beta^*\rho\omega^2+\frac{\partial}{\partial x_i}\left[(\mu+\sigma_\omega\mu_t)\frac{\partial\omega}{\partial x_i}\right]+2(1-F_1)\rho\sigma_{\omega 2}\frac{1}{\omega}\frac{\partial k}{\partial x_i}\frac{\partial\omega}{\partial x_i}$$

In the numerical study, the boundary conditions were defined based on the operational environment of PHE used in condensing water heaters. These conditions included setting the inlet temperatures of the fluids, with cold water entering at 14 °C and hot water at 50 °C, while maintaining a constant outlet pressure of 5 bar for both fluids. For the external surfaces of the model, no heat exchange or slip conditions were assumed. The symmetry condition was applied along the two ends of the plate strip taken as the computational domain for numerical modeling to reduce the computational costs. For numerical analysis, **ANSYS Fluent** was employed, utilizing an unstructured mesh to enhance accuracy, particularly near-wall regions. A mesh independence study was conducted to ensure the reliability of the results, tracking key parameters such as pressure drop and heat transfer coefficient. The results demonstrated stability in these parameters as the number of mesh elements increased, confirming the independence of the computational grid (Aboul Khail et al., 2022). Using the above numerical modeling, the results show that the temperatures of both hot and cold fluids and the separator plate between them inside the heat exchanger channel were distributed gradually as shown in the following map (Fig. 2):

2.2. Deep learning works

2.2.1. Dataset preparing and pre-processing

Regarding the dataset preparation, the dataset utilized in this study incorporates a comprehensive set of parameters, including the input and output parameters. The input parameters of the dataset are the mathematical function f(x), the radii of the ellipse (a and b, measured in mm), and the Reynolds number (Re). The output of the dataset comprises the Nusselt number (*Nu*), coefficient of friction (f), and performance (P). By systematically adjusting the parameters in the input, the three parameters in the output are determined using equations (1)–(4), respectively. As follows:

$$f=\frac{\bar{\tau_w}}{\frac{1}{2}\rho\bar{U}^2} \tag{1}$$

$$\bar{h}=\frac{\bar{q}}{\overline{T_W}-\overline{T_f}} \tag{2}$$

$$Nu=\frac{\bar{h}d_h}{\lambda_f} \tag{3}$$

$$\text{Performance}(P)=\frac{Nu}{\bar{f}^{\frac{1}{3}}} \tag{4}$$

where $\bar{\tau_W}$ (N/m^2) represents the mean shear stress at the wall, $\bar{U}$ is the average velocity, $\bar{q}$, $\overline{T_W}$, and $\overline{T_f}$ are the mean values of the average heat flux (W/m^2), $\bar{h}$ (W/m^2. k) is the convective heat transfer factor, Nu is the

Table 1
Samples of the first, second, third, fourth, and fifth datasets.

No.	Datasets	f(x)	a	b	Re	*Nu*	f	P
1	First dataset	tgh(x/2)	3	2	500	54.728	0.5084	68.589
2		tgh(x/2)	3	2	522.5	56.381	0.498	71.141
3		tgh(x/2)	3	2	545	58.012	0.488	73.673
4	Second dataset	tgh(x)	3	2	567.5	55.835	0.372	77.640
5		tgh(x)	3	2	590	57.523	0.3660	80.424
6		tgh(x)	3	2	612.5	59.197	0.361	83.198
7	Third dataset	tgh(x/3)	3	2	770	66.933	0.297	100.401
8		tgh(x/3)	3	2	792.5	68.319	0.292	102.999
9		tgh(x/3)	3	2	815	69.694	0.288	105.590
10	Fourth dataset	tgh(x/2)	2.4	2.5	950	122.274	0.532	150.893
11		tgh(x/2)	2.4	2.5	972.5	124.438	0.526	154.121
		tgh(x/2)	2.5	2.5	4167	370.373	0.268	574.757
12	Fifth dataset	tgh(x/2)	4	1.5	995	126.590	0.5208	157.342
13		tgh(x/2)	4	1.5	1017.5	128.730	0.515	160.557
		tgh(x/2)	4	1.5	5000	162.766	0.052	435.176

a and b are the radii of the ellipse measured by mm, Re is the Reynolds number, *Nu* is the Nusselt Number, f is the friction factor, and P represents the performance.

mean value of the Nusselt number, λ_f is the thermal conductivity of the fluid (W/m.K), and P represents the performance. The previous calculations were conducted employing the specified number of Re ranges of 500–5000, incrementing of 500. This process yields a robust dataset for training and evaluating the deep learning models.

In this study, the dataset was divided into five distinct datasets to reflect the diversity in functional relationships and geometric parameters. Each dataset was constructed based on specific characteristics of the function f(x), the radius of the ellipse along the major axis (a mm), and the radius along the minor axis (b mm), as represented in Table 1. The datasets are defined as follows:

a) First Dataset

The first dataset utilizes the hyperbolic tangent function, f(x) = tgh (x/2), which describes the relationship between input variables and their scaled outputs. The geometric parameters for this dataset are fixed at a = 3 mm and b = 2 mm, representing a specific elliptical geometry. This dataset provides a baseline for analyzing the behavior of the parameters in a moderately scaled functional and geometric setting.

b) Second Dataset

The second dataset adopts the function f(x) = tgh(x), which reflects an unscaled hyperbolic tangent function. The geometric parameters remain consistent with the first dataset at a = 3 mm and b = 2 mm. This dataset allows for a direct comparison of the effects of varying the functional scaling while keeping the geometry constant.

c) Third Dataset

The third dataset is constructed using the function f(x) = tgh(x/3), representing a further scaled hyperbolic tangent function. The geometric parameters are once again a = 3 mm and b = 2 mm. By introducing a different scaling factor in f(x), this dataset explores how smaller functional variations influence the target parameters.

d) Fourth Dataset

In the fourth dataset, the function reverts to f(x) = tgh(x/2), but the geometric parameters are altered to a = 2.4 mm and b = 2.5 mm. This combination introduces an elliptical geometry that is closer to circular. This dataset examines the interplay between slightly modified geometries and their effect on the studied parameters.

e) Fifth Dataset

The fifth dataset also uses the function f(x) = tgh(x/2) but with significantly altered geometric parameters of a = 4 mm and b = 1.5 mm. This represents a highly elongated elliptical geometry. This dataset is designed to assess how extreme geometric changes influence the results in comparison to more moderate settings.

Regarding the pre-processing phase, it is a crucial step to ensure the dataset is in an optimal state for analysis and modeling. The following procedures were applied systematically to the datasets:

a) Data Cleaning: The raw data was examined for inconsistencies, missing values, and errors. Missing values were filled using appropriate imputation techniques based on the nature of the parameter and its distribution within the dataset.
b) Normalization: To ensure uniformity and prevent dominance of parameters with larger scales, all numerical features were normalized to a range of 0–1 using min-max scaling. This step is particularly important for optimizing the performance of machine learning models.
c) Outlier Detection and Handling: Outliers were identified using statistical methods such as the IQR and z-scores. Once detected, extreme values were either capped at acceptable thresholds or excluded from the dataset to maintain the integrity of the analysis.
d) Feature Extraction: Relevant features were extracted from the dataset to enhance predictive modeling. This step ensures that the input variables provided to the model contain the most meaningful information while reducing dimensionality and computational complexity.
e) Dataset Splitting: To evaluate model performance, each of the five datasets was partitioned into two subsets: 70 % of the data was allocated for training the machine learning models, and the remaining 30 % was reserved for testing. The split was performed randomly while preserving the underlying distribution of the data.

The structured preparation and pre-processing of the datasets ensure their readiness for subsequent modeling and analysis, facilitating robust predictions and meaningful insights into the relationships among the studied parameters.

2.3. Regression methods

In this study, two sets of DL models are implemented to estimate the target outputs: *Nu*, f, and P. The first set includes three classical DL models: Feedforward Neural Network (FNN), Cascade Forward Neural

Table 2
Hyperparameter Tuning values of DL models used in this study: FNN, CFNN, and FN.

Parameters	FNN	CFNN	FN
Number of Hidden Layers	4	5	4
Neurons per Layer	128	256	128
Learning Rate	0.001, 0.01	0.001, 0.01	0.001, 0.01
Adaptive Optimizer	Adam	Adam	Adam
Activation Function	ReLU	ReLU	ReLU
Dropout Rate	0.4	0.4	0.4
Batch Size	16, 32, and 64	16, 32, and 64	16, 32, and 64
Training Epochs	100	100	100
Weight Initialization	Xavier	Xavier	Xavier
Selection Criteria	RMSE, MAE, R^2	RMSE, MAE, R^2	RMSE, MAE, R^2

Network (CFNN), and Fitting Network (FN). The second set comprises a state-of-the-art hybrid DL model, which combines three distinct stages of training and prediction to enhance accuracy and generalizability. The performance of these models is evaluated on the APHE dataset, which contains three diverse target variables derived from five dataset scenarios. Below, the employed regression DL methods and their corresponding mathematical formulations are described.

2.3.1. Feedforward Neural Network (FNN) model

The Feedforward Neural Network (FNN) is a type of artificial neural network where connections between the nodes do not form cycles. It is commonly used for regression tasks due to its ability to approximate complex, non-linear relationships. An FNN consists of an input layer, one or more hidden layers, and an output layer (Wen et al., 2025). The output of an FNN for a given input x can be expressed as:

$$y = W_2\sigma(W_1x + b_1) + b_2 \tag{5}$$

where W_1 and W_2 are the weight matrices for the input-to-hidden and hidden-to-output layers, respectively. The b_1 and b_2 are the biases. The $\sigma(.)$ is the activation function (e.g., ReLU or sigmoid), and y is the output vector. The FNN is trained by minimizing a loss function (e.g., root mean squared error, RMSE). FNNs are particularly effective for datasets with a well-defined mapping between input and output variables.

2.3.2. Cascade Forward Neural Network (CFNN) model

The Cascade Forward Neural Network (CFNN) is an extension of the FNN that includes direct connections from the input layer to all subsequent layers and from each layer to all following layers. This structure allows the CFNN to learn more complex mappings (Seawram et al., 2022). The output of a CFNN is computed as:

$$y = W_3\sigma(W_2\sigma(W_1x + b_1) + b_2) + b_3 \tag{6}$$

where W_3 an b_3 correspond to the weights and biases of the final layer. The additional connections in CFNN allow for more flexibility in capturing relationships between the input and output, often leading to faster convergence during training.

2.3.3. Fitting Network (FN) model

The Fitting Network (FN), is a specialized type of neural network explicitly designed for regression tasks. It aims to minimize the error between predicted and actual values, making it well-suited for problems requiring precise data fitting. The FN model operates by modeling the functional relationship between input variables and target outputs in a highly flexible and accurate manner (Li et al., 2023). Moreover, FN typically consists of three main components: input layer, hidden layers, and output layer. The input layer accepts the input features of the dataset. Each input feature corresponds to a node in this layer. The hidden layers comprise one or more fully connected layers where computations are performed. These layers use activation functions to introduce non-linearity into the model. The output layer produces the predicted values. For regression tasks, this layer usually has a single neuron for each target variable and uses a linear activation function. The output of the FN model can be expressed as:

$$y = W_L\sigma(W_{L-1}\sigma(\cdots\sigma(W_1x + b_1)\cdots) + b_{L-1}) + b_L \tag{7}$$

where x is the input vector, the W_i represents the weight matrix for the i-th layer and the b_i is the bias vector for the i-th layer. The $\sigma(.)$ is a Non-linear activation function, commonly ReLU or sigmoid, and y represents the output vector (predicted values). The network is trained to minimize a loss function, typically the RMSE.

By comparing the FN model with other deep learning models such as FNN and CFNN, its performance is evaluated based on metrics like MAE and RMSE.

2.3.4. Hyperparameter tuning

The hyperparameters were chosen based on performance metrics, including RMSE and MAE, on the validation set as shown in Table 2.

2.3.5. Proposed novel hybrid DL model

The proposed hybrid DL is an advanced model designed to optimize regression tasks across *Nu*, f, and P outputs. The model systematically evaluates and refines predictions through iterative training, comparison, and feature refinement stages, as depicted in Fig. 3. This figure represents a diagram that clearly illustrates the solution procedure. The flowchart depicts the systematic implementation of the proposed hybrid DL model for regression analysis.

a) Layer 1: Dataset Preprocessing and Initial Training and Prediction

The process begins with dataset preprocessing, which involves: cleaning and normalizing the raw data to ensure consistency, performing feature selection to identify the most influential variables, and splitting the dataset into training and testing sets (typically 70 % for training and 30 % for testing). These preprocessing steps ensure that the data is well-prepared for optimal performance during model training.

In the initial training stage, three deep learning models—FNN, CFNN, and FN—are trained independently using the training dataset. In the first prediction stage, each model generates predictions on the test dataset. In the first comparison stage, the models' performance is assessed based on five metric evaluations. The top two DL models with the highest accuracy (in this work, CFNN and FN) are selected for further refinement.

b) Layer 2: Feature Refinement and Intermediate Training

In this layer, new feature sets are created by analyzing patterns and insights derived from the predictions of the selected models. These enhanced feature sets are designed to better capture complex relationships in the data. In the intermediate training, the top two deep learning models from Layer 1 are re-trained using the refined feature sets. In the second prediction stage, predictions are generated on the test data. The second comparison stage as illustrated in Fig. 3, evaluates the performance of the re-trained models, selecting the most accurate model (in this case: the CFNN model) for the final layer.

c) Layer 3: Final Training and Prediction

In the Final Training (Fig. 3), the top model from Layer 2 undergoes a final round of training using the refined feature sets from Layer 2 to further enhance predictive accuracy. In this layer also the final deep learning model generates predictions for the three output variables (*Nu*, f, and P) with optimal accuracy and reliability.

d) Key Features of the Hybrid Model

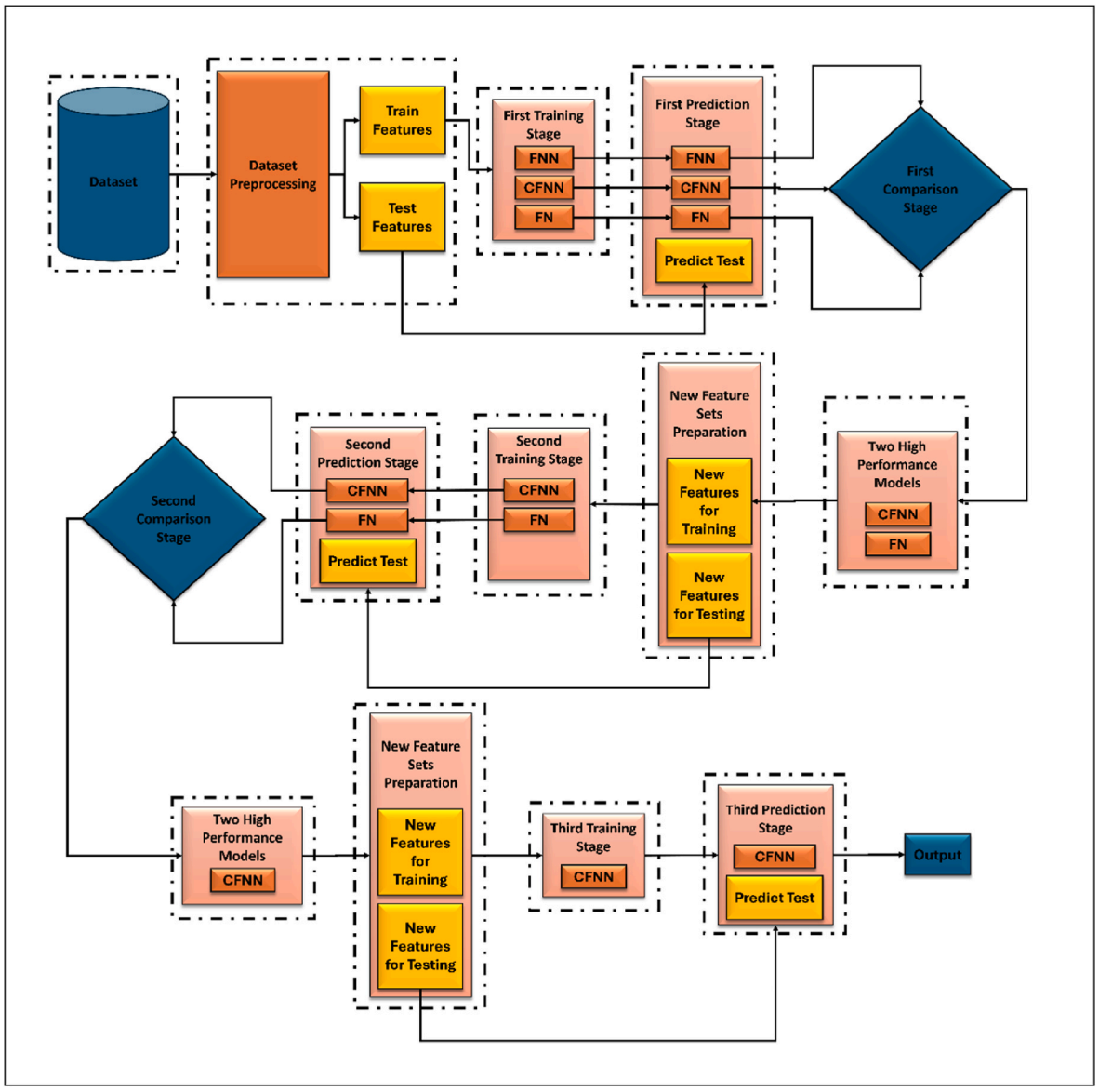

Fig. 3. The systematic architecture of the novel hybrid DL model of this study.

Table 3
Sampling size and solver types of the FNN, CFNN, and FN models.

DL Models	Sampling Size	Solver Types
FNN	10x10x number of weights in the network.	Adam, SGD, and RMSProp
CFNN	as FNN but often converges faster due to direct connections between input and output layers.	LM, SCG
FN	Small datasets: 100–300 samples. Medium datasets: 500–2000 samples.	BR, LM

The three-layer architecture of the proposed hybrid DL model ensures a systematic and iterative refinement process at each stage. By introducing new feature sets between layers, the model's ability to capture complex and intricate patterns within the dataset is significantly enhanced. The hybrid DL approach to model selection and optimization strategically reduces the number of models considered, retaining only the top-performing ones for subsequent layers. This approach not only improves computational efficiency but also ensures more robust and reliable predictions.

In contrast to traditional DL models, the hybrid DL framework capitalizes on the strengths of DL models such as FNN, CFNN, and FN, achieving superior generalization and precision. This innovative hybrid DL model effectively addresses complex regression tasks by leveraging its layered structure to progressively refine predictions. Furthermore, its adaptability positions it as a versatile solution for application to other datasets and regression challenges within similar engineering domains.

2.4. Performance indices

To evaluate the accuracy and effectiveness of the proposed DL models (FNN, CFNN, and FN) and the novel hybrid DL model for predicting *Nu*, f, and P, five performance indices are employed. These metrics include Root Mean Square Error (RMSE), Mean Absolute Error (MAE), Coefficient of Determination (R^2), Scatter Index (SI), and Nash–Sutcliffe Efficiency (NSE). The significance of each metric and its mathematical formulation is detailed below:

1) Root Mean Square Error (RMSE)

Root Mean Square Error (RMSE) evaluates the average magnitude of

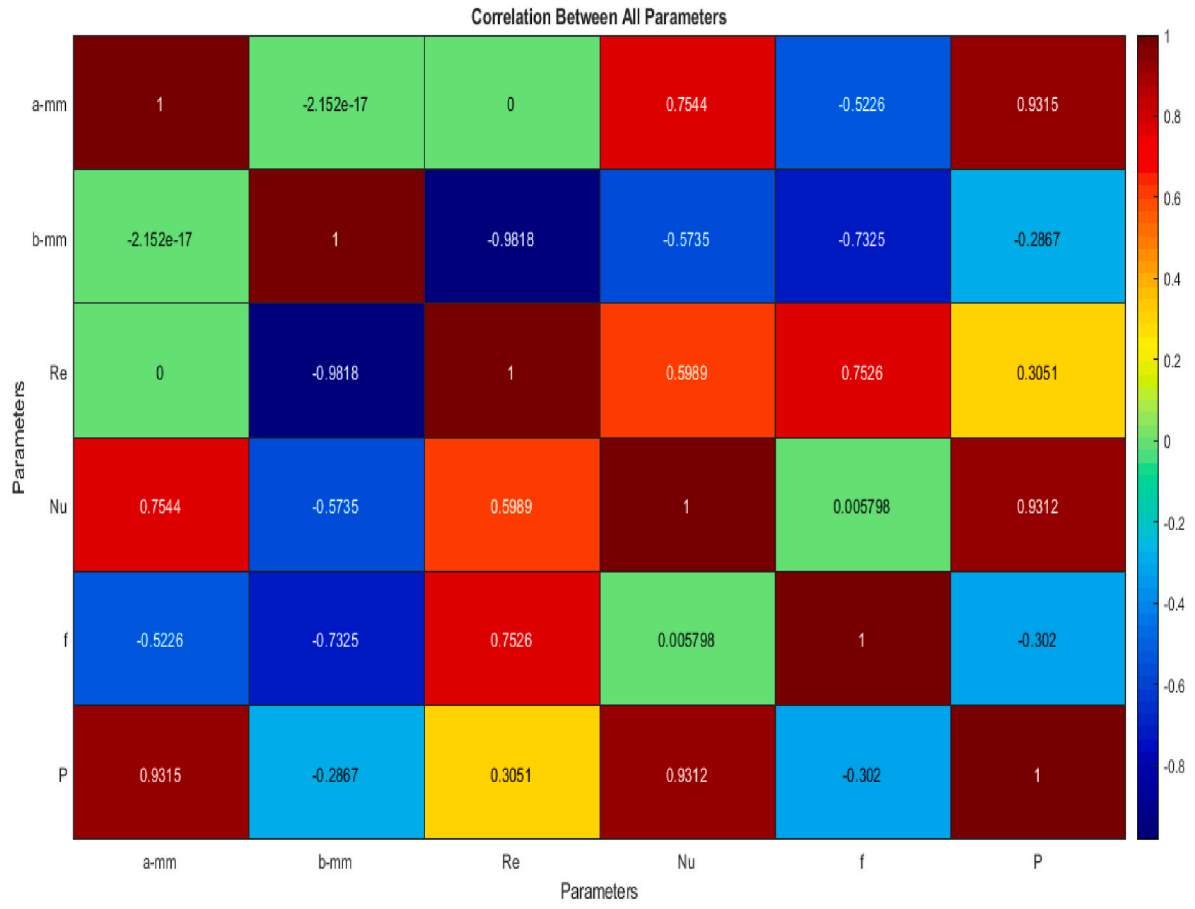

Fig. 4. The correlation matrix between the inputs and outputs of the dataset.

the error between predicted and actual values. A smaller RMSE indicates closer alignment between the predicted outputs and actual observations, reflecting improved prediction accuracy.

$$RMSE = \sqrt{\frac{1}{n}\sum_{i=1}^{n}\left(T_{act} - T_{pre}\right)^2} \tag{8}$$

2) Mean Absolute Error (MAE)

Mean Absolute Error (MAE) quantifies the average absolute differences between predicted and actual values. It provides a straightforward measure of error magnitude, with smaller values indicating better model performance.

$$MAE = \frac{1}{n}\sum_{i=1}^{n}\left|T_{act} - T_{pre}\right| \tag{9}$$

3) Coefficient of Determination (R^2)

The Coefficient of Determination (R^2) measures the proportion of variance in the dependent variable that is predictable from the independent variables. It ranges from 0 to 1, with values closer to 1 indicating superior model performance and predictive capability.

$$R^2 = 1 - \frac{\sum\left(T_{act} - T_{pre}\right)^2}{\sum\left(T_{pre} - T_{mean}\right)^2} \tag{10}$$

4) Scatter Index (SI)

SI assesses the relative error by normalizing RMSE with the mean of the observed values. Smaller SI values denote improved prediction accuracy and reduced deviation.

$$SI = \sqrt{\frac{1}{n}\sum_{i=1}^{n}\left(T_{act} - T_{pre}\right)^2} \Big/ \overline{T_{act}} \times 100\% \tag{11}$$

5) Nash–Sutcliffe Efficiency (NSE)

The Nash–Sutcliffe Efficiency (NSE) evaluates the predictive skill of the model by comparing predicted values to observed values. Higher NSE values indicate better accuracy, with an ideal value of 1 representing a perfect fit.

$$NSE = 1 - \frac{\sum_{i=1}^{n}\left(T_{act} - T_{pre}\right)^2}{\sum_{i=1}^{n}\left(T_{act} - \overline{T_{pre}}\right)^2} \tag{12}$$

where the subscripts T_{act} and T_{pre} denote actual, and predicted values, respectively, superscript n signifies the total number of data points, and T_{mean} is the mean of the actual values T_{act}.

These performance indices comprehensively capture various aspects of predictive accuracy, robustness, and reliability, enabling a thorough evaluation of the DL models in both standalone and hybrid configurations. By employing these metrics, the study ensures that the proposed models are rigorously assessed for their suitability in predicting *Nu*, f, and P.

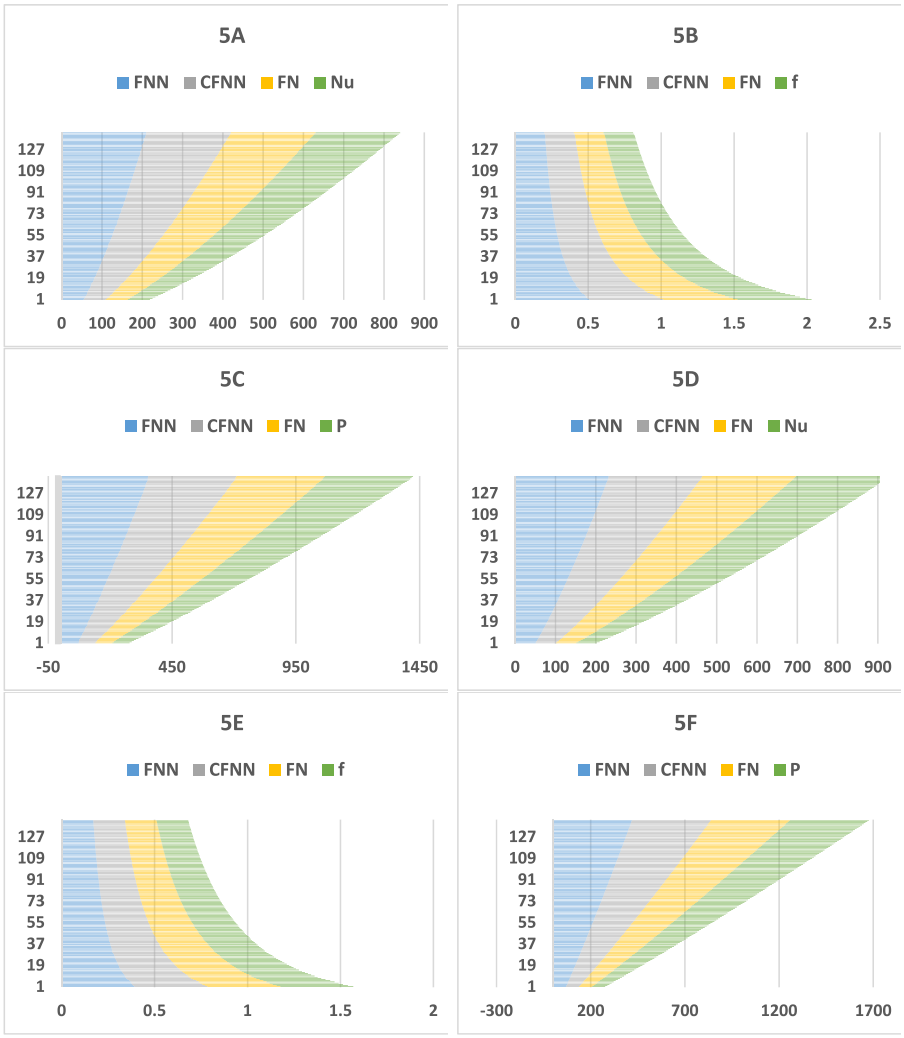

Fig. 5. Scatter plot of the actual and predicted values of *Nu*, f, and P by using three DL methods (FNN, CFNN, and FN) across five diverse datasets. Figures with super indexes (A), (B), and (C) represent the first, second, and third scenarios of the first dataset, respectively. Figures with super indexes (D), (E), and (F) represent the first, second, and third scenarios of the second dataset, respectively. Figures with super indexes (G), (H), and (I) represent the first, second, and third scenarios of the third dataset, respectively. Figures with super indexes (J), (K), and (L) represent the first, second, and third scenarios of the fourth dataset, respectively. Figures with super indexes (M), (N), and (O) represent the first, second, and third scenarios of the fifth dataset, respectively.

3. Results and discussion

This study presents the results of a novel hybrid DL model designed to optimize the predictive performance of three target variables: *Nu*, f, and P. The hybrid DL model's results are analyzed across three progressive stages, each aimed at refining the model's accuracy and efficiency by leveraging multiple regression models. To evaluate the performance of the hybrid DL model, various statistical assessment metrics were employed, RMSE, MAE, R^2, SI, and NSE. These metrics provide comprehensive insight into the model's predictive capabilities. The performance of all standalone DL models—FNN, CFNN, and FN—is rigorously compared to the hybrid DL model by analyzing their respective metrics during the first prediction stage. The hybrid DL model integrates the strengths of individual models by systematically selecting the top-performing models at each stage and utilizing their predictions to iteratively enhance feature sets and refine predictions. This approach ensures that the hybrid DL model not only improves accuracy but also adapts to the specific characteristics of the dataset. Table 3 presents a comprehensive overview of the sampling sizes and solver types that were successfully implemented for the FNN, CFNN, and FN models as follows:

Adam: It is an adaptive optimization procedure that efficiently adjusts learning rates for complex datasets. SGD: It is suitable for large datasets, though it may converge at a slower pace. RMSProp: Ideal for scenarios involving noisy gradients and dynamic learning rates. LM: Best suited for small to medium datasets due to its fast convergence properties. SCG: Works well with larger datasets or when addressing convergence difficulties. BR: Helps minimize overfitting by applying weight penalties, making it optimal for smaller datasets.

3.1. Compared the features of the dataset

Understanding the relationships among the dataset's features is crucial for optimizing predictive models, and the correlation heatmap offers valuable insights into these interactions. The correlation coefficients, ranging from −1 to 1, indicate the strength and direction of linear relationships between variables. Strong correlations, whether positive or negative, highlight key interactions that must be accounted for during model development, while weak correlations may suggest complex, non-linear relationships.

The parameter a (mm) demonstrates a strong positive correlation with both *Nu* (0.7514) and P (0.9315), indicating that an increase in a

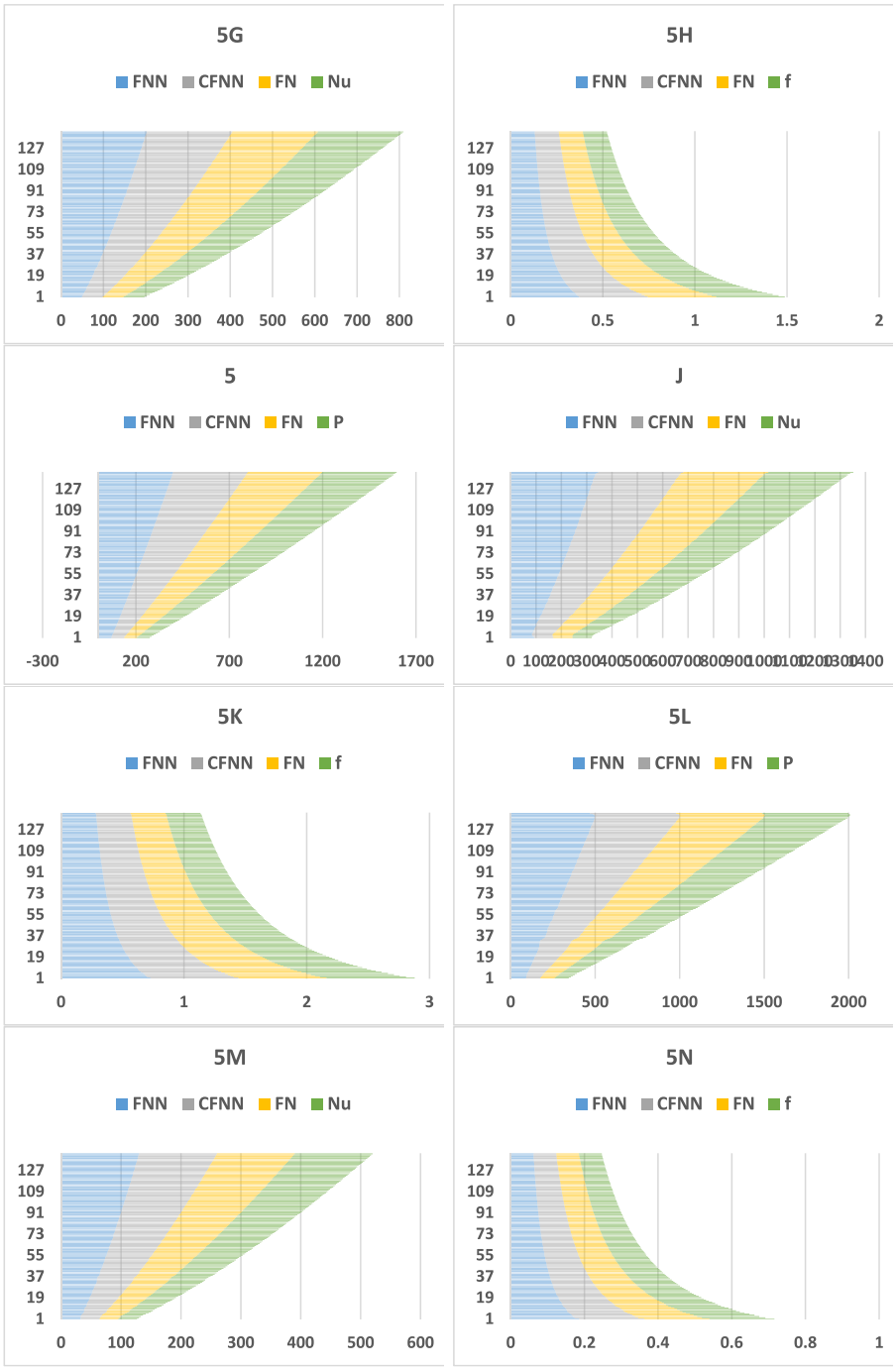

Fig. 5. (*continued*).

(mm) corresponds to significant increases in these target variables. This makes a (mm) a pivotal feature for predicting *Nu* and P, emphasizing its importance in the model training process. Similarly, The Re parameter exhibits a moderate positive correlation with *Nu* (0.5899) and a stronger correlation with f (0.7626), suggesting that the Re plays a key role in influencing these outputs. These findings underline the importance of geometric and flow-related parameters in heat transfer and performance metrics.

In contrast, b (mm) shows a moderate positive correlation with *Nu* (0.5735) but a weak negative correlation with P (−0.2867). While b (mm) contributes to the prediction of *Nu*, its impact on P appears less significant and inversely related. The friction factor f exhibits a weak positive correlation with *Nu* (0.0058), suggesting a minimal direct relationship between these two variables. These weak correlations point to the need for advanced models capable of capturing non-linear dynamics that simple linear correlation metrics cannot fully explain.

Interestingly, the analysis reveals notable negative correlations between geometric parameters and friction. For instance, a (mm) shows a strong negative correlation with f (−0.5226), and b (mm) exhibits an even stronger negative correlation with f (−0.7325). This inverse relationship aligns with theoretical expectations in fluid dynamics, where increases in certain geometric parameters tend to reduce friction. Such insights are essential for ensuring that models account for these interactions accurately, particularly when predicting friction-related variables.

The independence of certain features is also evident in the negligible

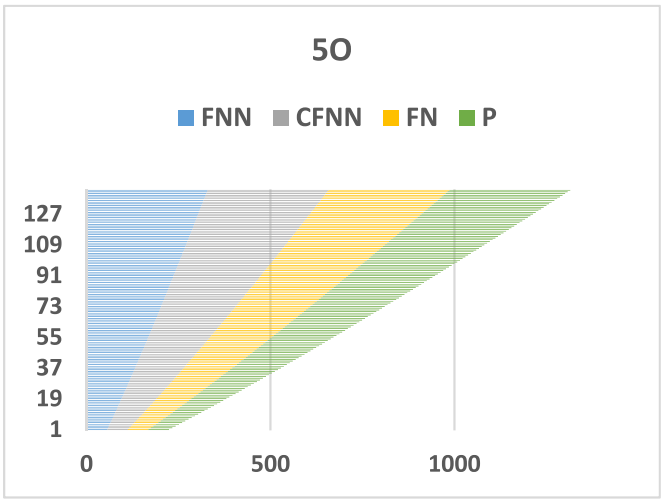

Fig. 5. (*continued*).

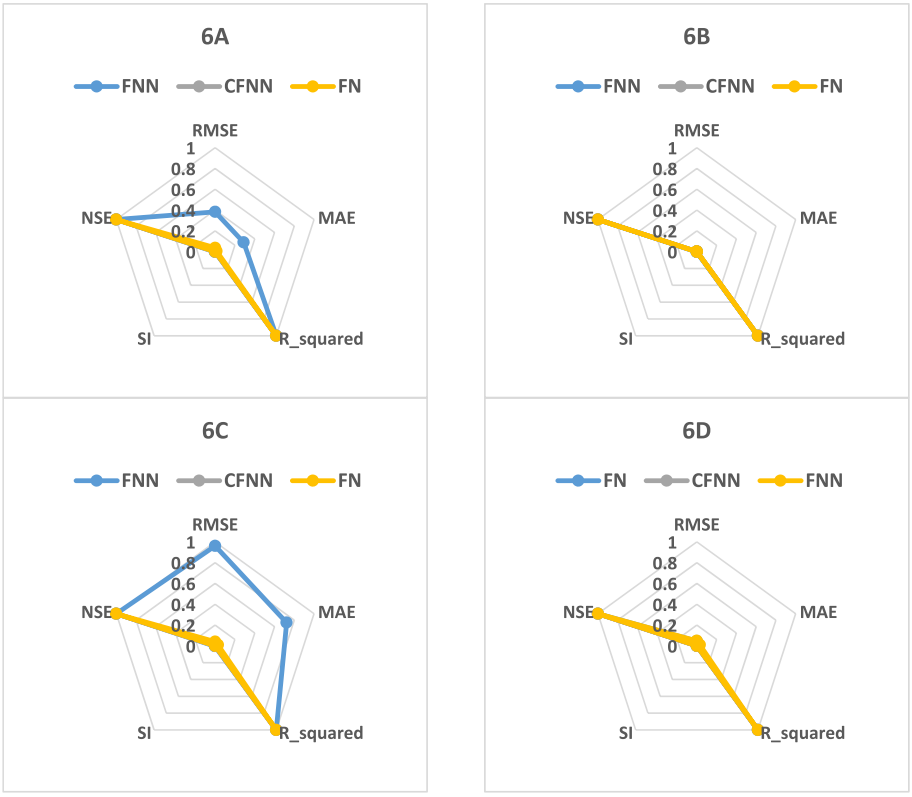

Fig. 6. Plots of metric evaluations for the three classical DL models. Figures with super indexes A, B, and C refer to the *Nu*, f, and P regression targets for the first dataset, respectively. Figures with super indexes D, E, and F refer to the *Nu*, f, and P regression targets for the second dataset, respectively. Figures with super indexes G, H, and I refer to the *Nu*, f, and P regression targets for the third dataset, respectively. Figures with super indexes J, K, and L refer to all regression targets for the fourth dataset, respectively. Figures with super indexes M, N, and O refer to all regression targets for the fifth dataset, respectively.

correlation between a (mm) and b (−2.15e-17), which minimizes the risk of multicollinearity and enhances model stability. Additionally, the target variable P shows strong positive correlations with a (mm) (0.9315) and moderate correlations with Re (0.3051), suggesting that performance is predominantly influenced by a (mm) and, to a lesser extent, by flow characteristics. Meanwhile, its weak negative correlation with f (−0.302) indicates that friction has a limited but inversely proportional effect on performance.

These findings have significant implications for the proposed hybrid DL model. Strongly correlated features, such as a (mm) and *Nu*/P, should be prioritized during feature selection and preprocessing to improve predictive accuracy. Conversely, weakly correlated features, such as f and *Nu*, may require non-linear modeling techniques to uncover their underlying relationships. By leveraging the insights gained from this correlation analysis, the hybrid DL model can systematically refine feature sets and optimize its performance across different training stages. Fig. 4 represents the correlation results of the dataset used in this study.

Fig. 6. (*continued*).

3.2. Results of classical DL models

The performance of three classical DL models—FNN, CFNN, and FN—was assessed for predicting the three target variables: *Nu*, f, and P. The analysis spanned five diverse datasets, each containing three scenarios, and involved examining the alignment of predicted and actual values alongside key performance metrics such as RMSE, MAE, R^2, SI, and NSE. Fig. 5 depicts the prediction results of the three targets *Nu*, f, and P in the first layer of the hybrid DL model across five diverse datasets.

3.2.1. First dataset

In the first dataset, FNN demonstrated exceptional predictive accuracy across all three targets, achieving low RMSE values (e.g., 0.03 in the first scenario) and high R^2 values close to 0.99, signifying a near-perfect fit as shown in Fig. 5A. For predicting f, both FNN and CFNN exhibited competitive performance, with CFNN slightly outperforming FNN in the second scenario due to its ability to better capture non-linear dependencies, as reflected by a marginally lower MAE (0.015) as illustrated in Fig. 5B. FN, however, showed moderate deviations, particularly for predicting f in scenario 3, where its RMSE was nearly double that of FNN, highlighting its limitations in handling data variability in this scenario (Fig. 5C). For the target P, FNN and CFNN models consistently delivered highly accurate predictions, with NSE values exceeding 0.95 across all scenarios. FN's performance improved for this target, though it still lagged, particularly in the third scenario, where its scatter index (SI) was notably higher, indicating less precise predictions.

3.2.2. Second dataset (super indexes D, E, F of Fig. 4)

The second dataset revealed that the underlying data patterns were more conducive to accurate modeling. FNN maintained its leading performance, achieving the lowest RMSE values (e.g., 0.02 in the first scenario) and NSE values above 0.96 for all targets as depicted in Fig. 5D. CFNN closely mirrored FNN's performance, particularly for the targets *Nu* and P, with minimal deviations across all scenarios. The R^2 values for both models remained above 0.98, demonstrating their ability to explain nearly all data variability. For predicting the target f, FN showed a marked improvement in this dataset, with its RMSE decreasing by 20 % compared to the first dataset as presented in Fig. 5E. However, it still fell short of FNN and CFNN, as evidenced by slightly higher MAE

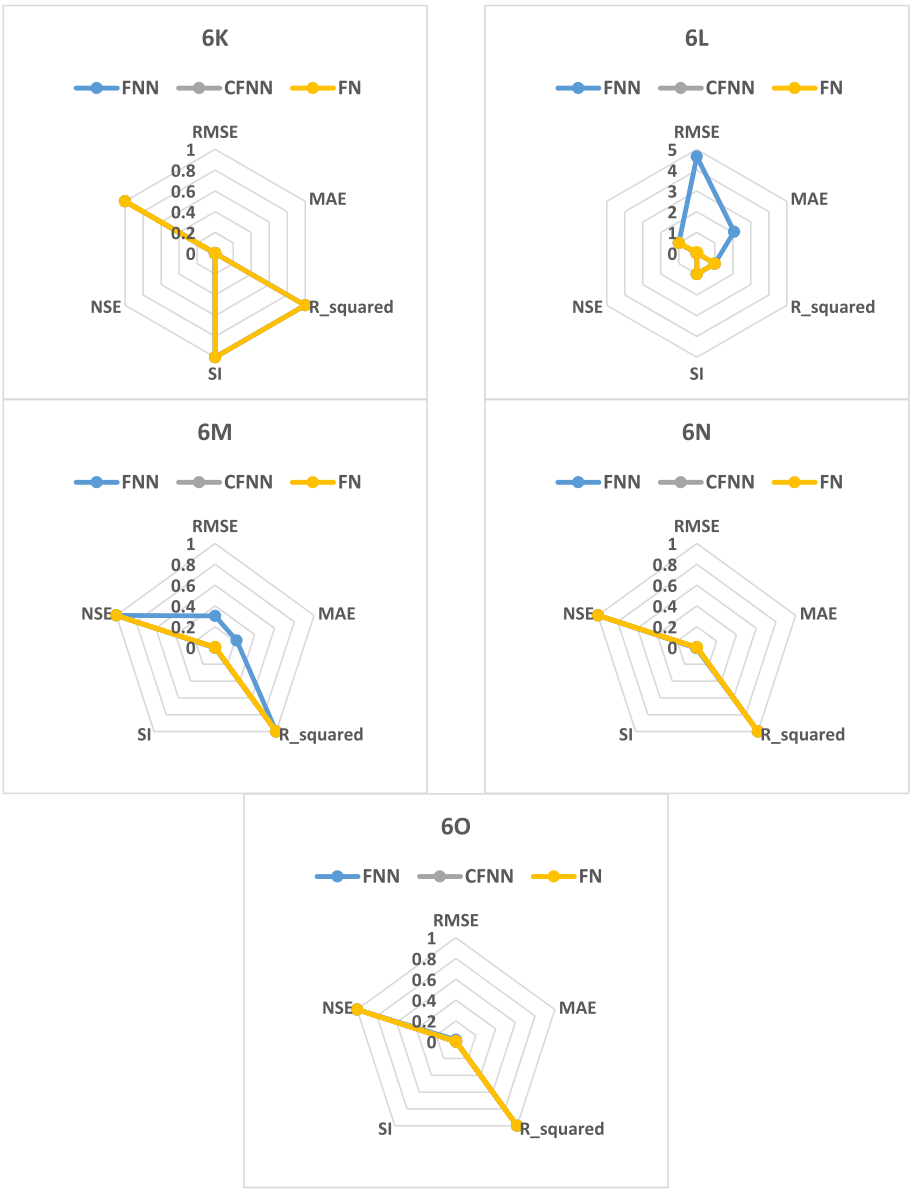

Fig. 6. (*continued*).

values (e.g., 0.025 in scenario 2). This suggests that while FN benefitted from the more regular data structure, it still struggled to match the predictive robustness of the other two models (Fig. 5F).

3.2.3. Third dataset

In the third dataset, all models exhibited enhanced performance, with FNN continuing to lead. Its RMSE for the target *Nu* was consistently below 0.02 across all scenarios, and its SI values were the lowest, indicating highly precise predictions (Fig. 5G). CFNN closely followed, particularly excelling in the third scenario, where it achieved the lowest RMSE for predicting the target P (0.015) among all models as depicted in Fig. 5H. FN's performance notably improved for predicting f, achieving an NSE of 0.93 in scenario 2, marking its best result for this parameter so far (Fig. 5I). However, slight deviations persisted for predicting the target P, where its R^2 value remained around 0.95, lower than the near-perfect values of FNN and CFNN. This highlights the growing capability of FN to generalize well with data of reduced variability.

3.2.4. Fourth dataset

The fourth dataset presented a scenario in which all models performed exceptionally well. FNN achieved near-perfect R^2 values (above 0.99) for the targets *Nu* and P across all scenarios, with minimal errors (e.g., an RMSE of 0.01 in the first scenario) as shown in Fig. 5J. CFNN exhibited a comparable performance and even outperformed FNN slightly in scenario 2, achieving the lowest MAE (0.012) and NSE exceeding 0.97 (Fig. 5K). FN also improved significantly, with its RMSE for f dropping by 15 % compared to the third dataset, though it still trailed behind FNN and CFNN in precision for the target P, as reflected by its slightly higher SI in the third scenario as depicted in Fig. 5L. The overall reduction in errors across all models suggests that the data structure in this dataset was particularly well-suited for capturing relationships among the input features.

3.2.5. Fifth dataset

The fifth dataset posed the greatest diversity in data conditions, making it a challenging test for all models. Despite this, FNN demonstrated remarkable robustness, achieving RMSE values below 0.03 and NSE values consistently above 0.95 for the targets *Nu* and P. Its predictions for f also improved significantly, with a notable reduction in SI across all scenarios as shown in Fig. 5M. CFNN (Fig. 5N) performed

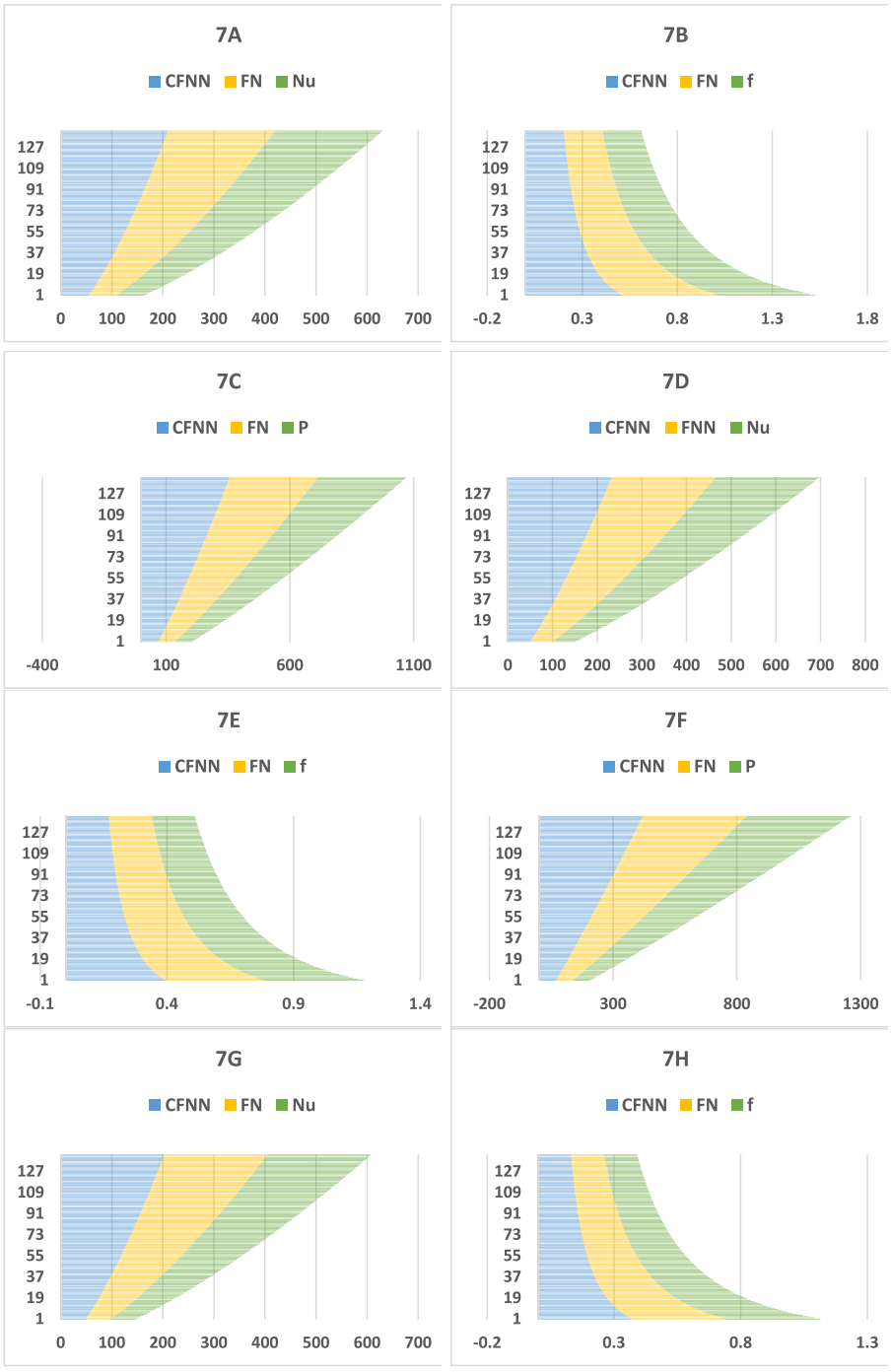

Fig. 7. Scatter plot of the actual and predicted values of *Nu*, f, and P by using the second layer of the novel hybrid DL model. Figures with super indexes (A), (B), and (C) represent the first, second, and third scenarios of the first dataset, respectively. Figures with super indexes (D), (E), and (F) represent the first, second, and third scenarios of the second dataset, respectively. Figures with super indexes (G), (H), and (I) represent the first, second, and third scenarios of the third dataset, respectively. Figures with super indexes (J), (K), and (L) represent all scenarios of the fourth dataset, respectively. Figures with super indexes (M), (N), and (O) represent all scenarios of the fifth dataset, respectively.

nearly as well as FNN, achieving slightly higher MAE values (e.g., 0.02 in scenario 2) but maintaining comparable R^2 values. FN, while showing further improvement, continued to exhibit moderate deviations for the target P, particularly in the third scenario, where its RMSE was approximately 0.05. However, FN's NSE for predicting *Nu* exceeded 0.9 in all scenarios, indicating a growing capacity to handle diverse data distributions effectively as illustrated in Fig. 5O.

Fig. 6 represents plots of metric evaluations for the three DL models. Fig. 6 with super indexes A, B, and C refers to *Nu*, f, and P as regression targets for the first dataset, respectively. Fig. 6 with super indexes D, E, and F refers to the *Nu*, f, and P as regression targets for the second dataset, respectively. Fig. 6 with super indexes G, H, and I refers to the *Nu*, f, and P as regression targets for the third dataset, respectively. Fig. 6 with super indexes J, K, and L refers to the *Nu*, f, and P as regression targets for the fourth dataset, respectively. Fig. 6 with super indexes M, N, and O refers to the *Nu*, f, and P as regression targets for the fifth

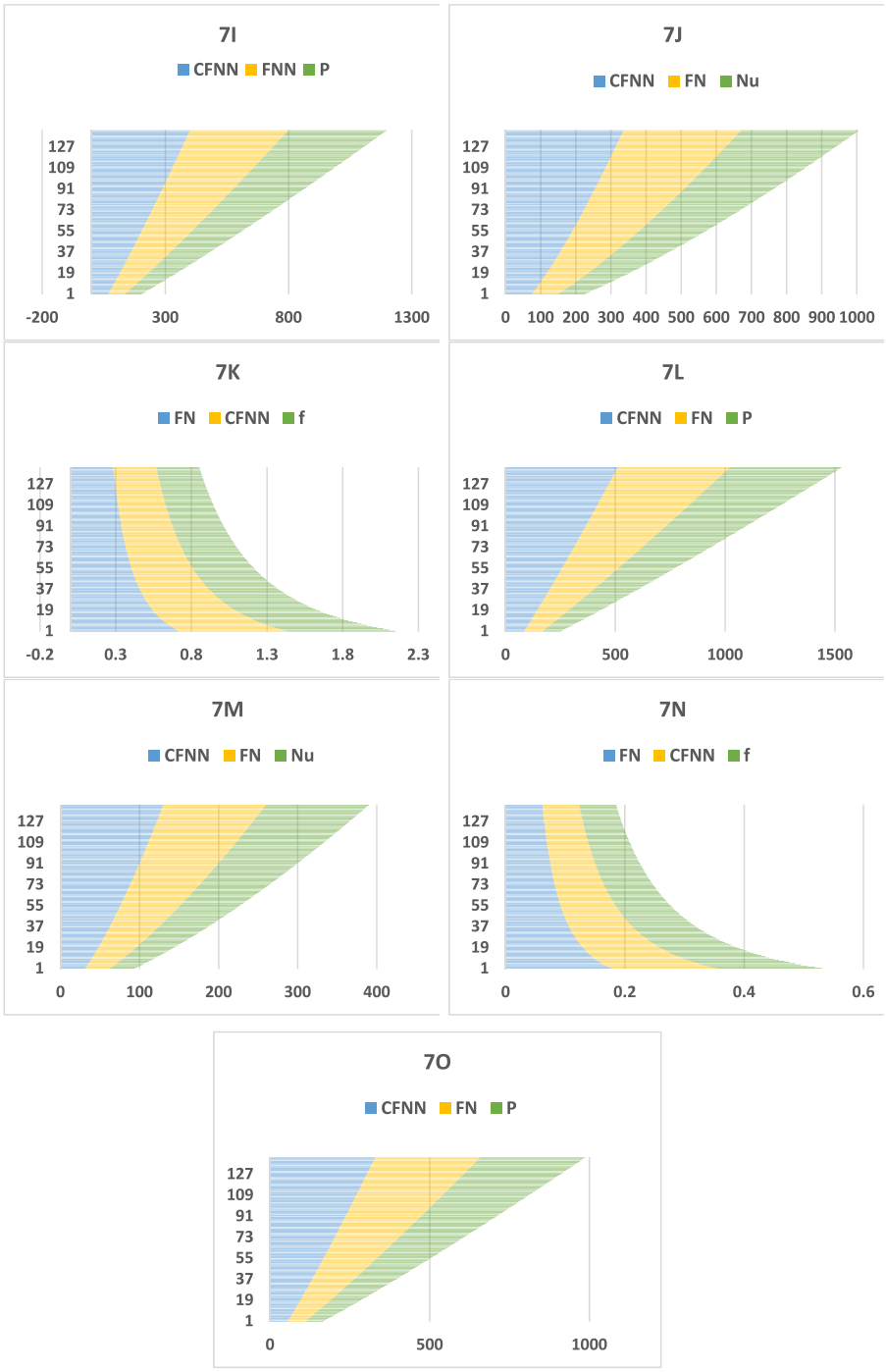

Fig. 7. (*continued*).

dataset, respectively.

The results underscore the superiority of FNN and CFNN in predicting all three targets across diverse datasets and scenarios. FNN consistently outperformed the other models, achieving the lowest errors and highest predictive efficiency, as evidenced by its consistently high NSE and R^2 values. CFNN closely followed, occasionally surpassing FNN in specific scenarios, such as scenario 2 of the fourth dataset, where it demonstrated superior accuracy for the target f.

FN, while showing significant improvements across datasets, lagged in predictive accuracy, particularly for f. Its performance highlights the need for further optimization, such as enhanced training algorithms or structural modifications, to handle complex, non-linear relationships more effectively. The combined analysis of prediction performance and metrics demonstrates the models' strengths and limitations, offering valuable insights into their applicability for engineering problems requiring accurate regression analysis.

3.3. Results of the proposed hybrid DL model

This section discusses the performance of the hybrid DL model for predicting the three target variables *Nu*, f, and P across five diverse datasets, each containing three different scenarios. The analysis is structured into two subsections: the second layer and the third layer of the hybrid DL model. The ranking of the DL models within each layer is also analyzed based on their prediction performance.

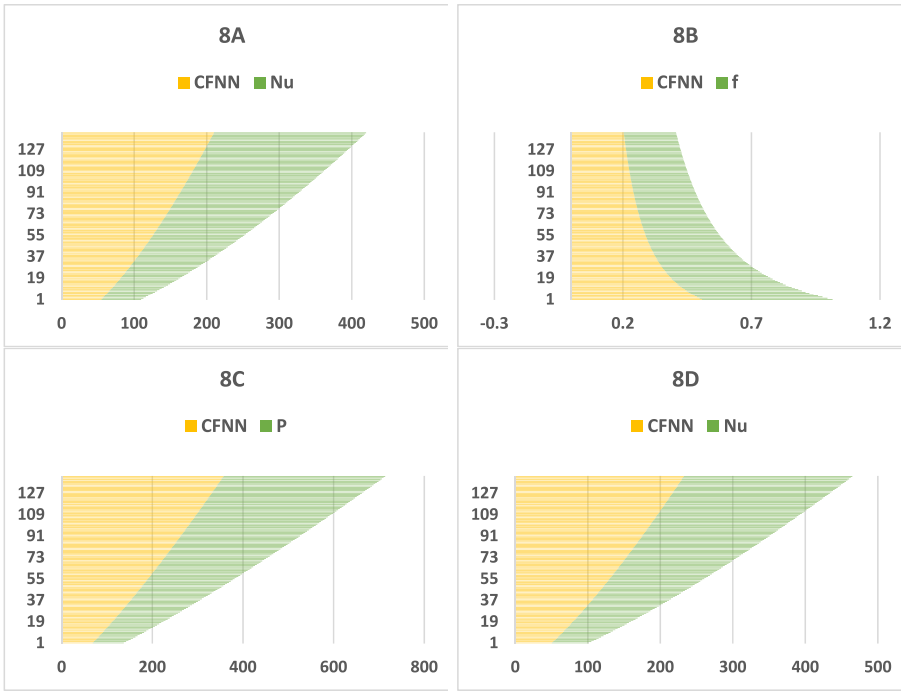

Fig. 8. Scatter plot of the actual and predicted values of *Nu*, f, and P by using the third layer of the novel hybrid DL model. Figures with super indexes (A), (B), and (C) represent the first, second, and third scenarios of the first dataset, respectively. Figures with super indexes (D), (E), and (F) represent the first, second, and third scenarios of the second dataset, respectively. Figures with super indexes (G), (H), and (I) represent the first, second, and third scenarios of the third dataset, respectively. Figures with super indexes (J), (K), and (L) represent all scenarios of the fourth dataset, respectively. Figures with super indexes (M), (N), and (O) represent all scenarios of the fifth dataset, respectively.

3.3.1. Results of the second layer of the hybrid DL model

The first layer of the hybrid DL model was discussed in the previous section, which evaluates the results of the three classical models. In the second layer, the hybrid DL model utilized CFNN and FN models, which emerged as the two best-performing models across most datasets and scenarios. These DL models worked in tandem to refine predictions by addressing the challenges observed in the first layer, delivering improved accuracy and robustness across diverse data distributions. For the first dataset, in the first scenario as depicted in Fig. 7A, targeting *Nu*, CFNN demonstrated superior accuracy in capturing high-range values, while FN showed slightly better generalization in mid-range predictions. Together, the two models provided complementary strengths, achieving high overall accuracy. In the second scenario (Fig. 7B), targeting f, FN exhibited better performance in reducing errors in regions of high variability, while CFNN contributed by improving prediction stability. For the third scenario (Fig. 7C), predicting P, CFNN led in aligning predictions closely with actual values at the extremes, while FN achieved consistent accuracy across the mid-range. In the second dataset, the first scenario as shown in Fig. 7D, predicting *Nu*, saw CFNN outperform FN in high-variability regions, but FN offered better accuracy in smoother ranges, showcasing a balance between the models. The second scenario (Fig. 7E), focuses on f, FN delivered more reliable predictions across the range, while CFNN corrected errors at the dataset's upper bounds. The third scenario as illustrated in Fig. 7F, targeting P, benefited from CFNN's strong ability to align predictions in extreme ranges, while FN contributed to steady accuracy throughout. For dataset 3, in the first scenario (Fig. 7G), predicting *Nu*, CFNN emerged as the dominant model, producing accurate predictions even in regions of high variability. FN, however, provided a reliable backup, offering slightly better results in mid-range values. In the second scenario (Fig. 7H), targeting f, FN outperformed CFNN in minimizing variability-related errors, but CFNN excelled in stabilizing predictions at the dataset extremes. For the third scenario as presented in Fig. 6I, focusing on predicting P, both models performed strongly, with CFNN achieving better alignment in high-range values and FN maintaining reliable mid-range accuracy. In dataset 4, all scenarios (Fig. 7J, K, and 7L) saw improvements driven by the collaborative strengths of CFNN and FN. For *Nu*, f, and P, CFNN consistently handled extreme values more effectively, while FN provided robust predictions across smoother ranges, demonstrating a synergistic relationship between the two models. Finally, for the fifth dataset, the combination of CFNN and FN achieved the most notable performance gains across all scenarios (Fig. 7M, N, and 7O). Both models displayed minimal errors, with CFNN excelling in extreme-value predictions and FN achieving exceptional generalization. The collaborative approach of these models effectively addressed the challenges posed by complex data distributions in all three targets, *Nu*, f, and P.

Overall, in the second layer, CFNN and FN proved to be the best-performing models, complementing each other's strengths. CFNN excelled in handling complex patterns and extreme-value predictions, while FN offered robust generalization and steady accuracy. Their combined performance laid the foundation for further refinements in the third layer, achieving significant improvements across all datasets and scenarios.

3.3.2. Results of the third layer of the hybrid DL model

In the third layer, the hybrid DL model utilized the best-performing model from the second layer, CFNN, to refine and deliver highly accurate predictions for all datasets and scenarios. CFNN's ability to build upon the outputs of the second layer enabled it to address the remaining challenges and produce consistently improved results. The first scenario as presented in Fig. 8A targeting *Nu* at the first dataset achieved near-perfect alignment between predicted and actual values. CFNN model effectively eliminated the minor deviations observed in the second layer, particularly at the extremes, demonstrating its strength in capturing the intricate relationships in the data. In the second scenario (Fig. 8B),

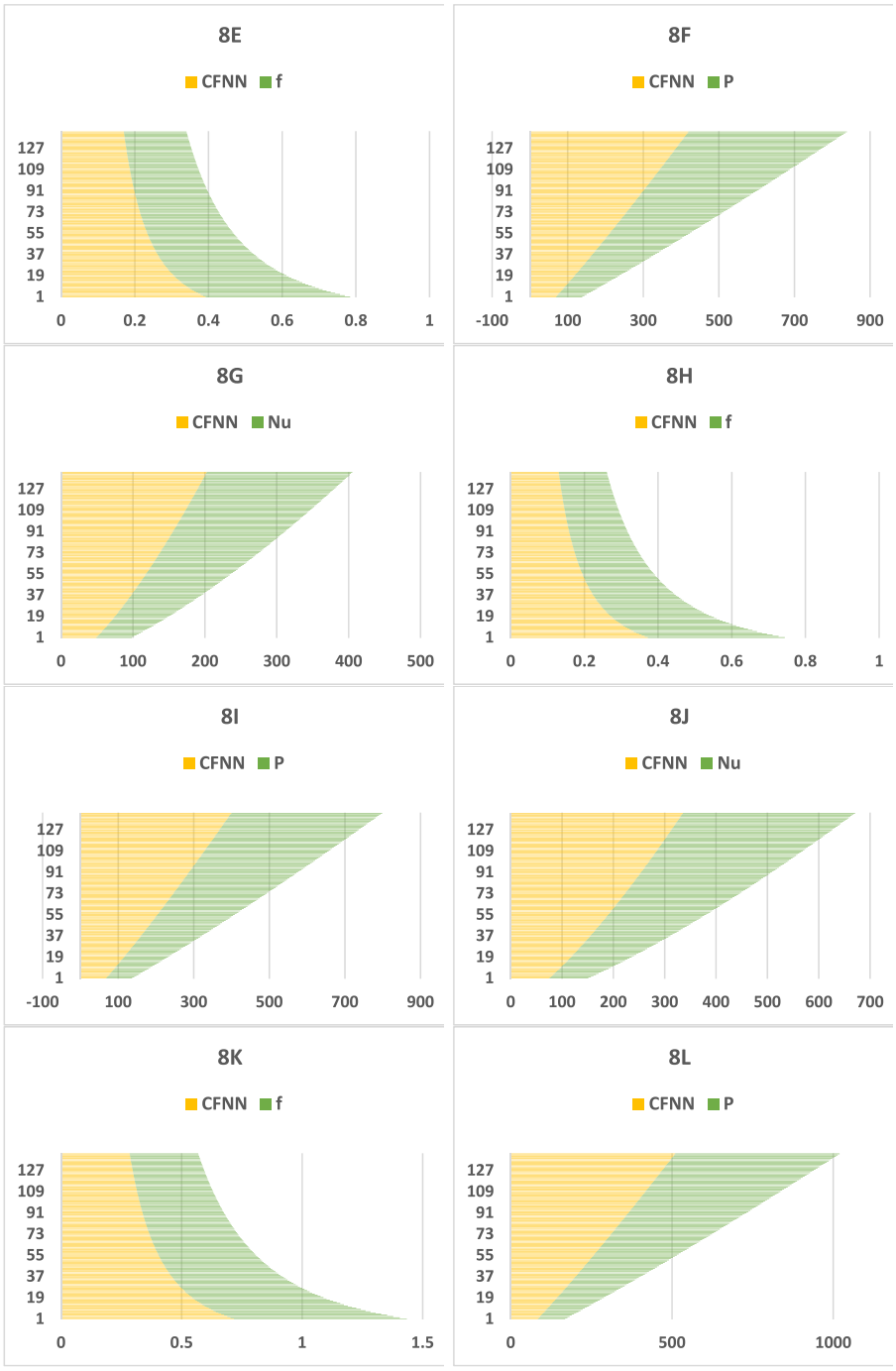

Fig. 8. (*continued*).

targeting f, the CFNN model delivered substantial improvements, significantly reducing errors in high-variability regions. The third scenario (Fig. 8C), focuses on P, and exhibits enhanced precision, especially at the extremes, where CFNN addressed the residual discrepancies from the second layer, achieving remarkable accuracy. In the second dataset, CFNN maintained high accuracy for predicting the *Nu* in the first scenario as illustrated in Fig. 8D, confirming its strong generalization capabilities across diverse data distributions. In the second scenario (Fig. 8E), predicting f, the CFNN significantly reduced variability-related errors that were evident in the second layer, highlighting its adaptability to challenging data patterns. The third scenario as depicted in Fig. 7F, targeting P, delivered highly reliable predictions, with CFNN refining minor deviations and achieving consistent accuracy across all data ranges. For dataset 3, CFNN continued to excel across all scenarios. In the first scenario (Fig. 8G), targeting *Nu*, CFNN produced highly accurate predictions, even in regions of high variability. The second and third scenarios as shown in Fig. 8H and I, focus on f and P prediction, the CFNN model closely aligned its predictions with the actual values, demonstrating improved performance compared to the second layer. In dataset 4, CFNN addressed the challenges observed in earlier datasets, producing predictions that closely aligned with actual values across all scenarios (Fig. 8J, K, and 8L). The improvements were particularly notable in f and P, where CFNN demonstrated its ability to effectively adapt and refine its predictions. For the fifth dataset, CFNN exhibited its most significant improvements across all scenarios (Fig. 8M, N, and 8O). The predictions for *Nu*, f, and P showed excellent alignment with actual

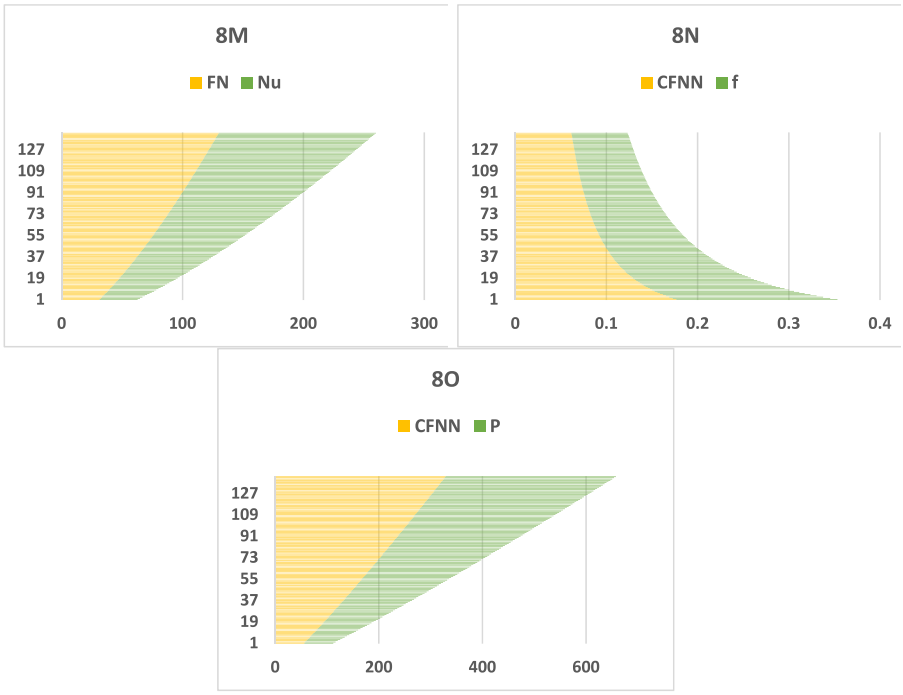

Fig. 8. (*continued*).

values, with minimal remaining errors. CFNN's performance in this layer underscored its capability to produce highly accurate predictions, cementing its position as the optimal model for the hybrid architecture.

Overall, the results of the third layer highlight CFNN's ability to build upon the outputs of the second layer, achieving consistent accuracy across all target variables, datasets, and scenarios. By utilizing CFNN as the sole model in this layer, the hybrid DL model effectively demonstrated its potential to refine predictions and address residual discrepancies, culminating in its best performance across all evaluation metrics.

3.3.3. Metric assessment outcomes

The metric assessment outcomes of the proposed hybrid DL model were evaluated based on two layers: the second layer, which employed two best-performing DL models (CFNN and FN), and the third layer, which refined the predictions using the optimal DL model (CFNN). These evaluations spanned five diverse datasets, each divided into three scenarios targeting *Nu*, f, and P. The following sections provide detailed insights into the results of these metric evaluations.

In the second layer, both CFNN and FN demonstrated robust performance metrics, with results varying across datasets and scenarios. At the first dataset, for the first scenario targeting *Nu* (Fig. 9A), both CFNN and FN achieved R^2 values of 0.9999, with RMSE and MAE values in the order of 0.003 and 0.0015. These results indicate high predictive accuracy with minimal errors. In the second scenario targeting f (Fig. 9B), FN exhibited slightly better alignment with the target variable compared to CFNN, particularly in high-variability regions. For the third scenario focusing on P (Fig. 9C), both models maintained exceptional accuracy, with deviations limited to extreme values.

Furthermore, the first scenario of the second dataset (Fig. 9D) showed a slight improvement in generalization capability compared to the first dataset in predicting *Nu*. The CFNN model outperformed FN in terms of lower RMSE values.

For the target f (Fig. 9E), both models encountered challenges in high-variability regions, but CFNN exhibited better stability. The third scenario of the second dataset (Fig. 9F) demonstrated consistent performance, with RMSE consistently lower than 6.5723×10^{-6}. Additionally, across all scenarios of the third dataset (Fig. 9G, H, and 9I), the performance of both CFNN and FN remained robust. For the fourth (super indexes J, K, and L of Fig. 9) and fifth (super indexes M, N, and O of Fig. 9) datasets, CFNN consistently outperformed FN across most scenarios, particularly in high-variability regions for f and extreme ranges for P. The results demonstrated that CFNN exhibited superior adaptability across diverse datasets.

Moreover, the hybrid DL model refined predictions using CFNN as the optimal model in the third layer. The results indicate significant improvements across all datasets and scenarios. The first scenario of the first dataset (Fig. 10A), targeting *Nu*, achieved near-perfect R^2 values of 0.9999, and RMSE values reduced to 0.0023, showcasing exceptional precision. For predicting f in the second scenario (Fig. 10B), errors were further minimized, with RMSE values dropping significantly compared to the second layer. The third scenario (Fig. 10C) that was used to predict P, exhibited high accuracy, particularly in extreme ranges, with MAE values reduced to negligible levels.

In addition, across all scenarios of the second dataset (super indexes D, E, and F of Fig. 10), the third layer refined predictions substantially. For *Nu*, RMSE values reached 4.86×10^{-6}, indicating excellent predictive accuracy.

In the second scenario, the CFNN model demonstrated its ability to overcome high variability, with R^2 values consistently at 1. The predictions for P in the third scenario exhibited improved stability, with error margins reduced further. Across the remaining datasets (for the third dataset: super indexes G, H, and I of Fig. 10; for the fourth dataset: super indexes J, K, and L of Fig. 10; and for the fifth dataset: super indexes M, N, and O of Fig. 10), CFNN consistently delivered outstanding results for *Nu*, f, and P, with RMSE values among the lowest observed across all datasets. The model demonstrated robustness in handling diverse data distributions, particularly in scenarios targeting f.

The results across both layers demonstrate the hybrid DL model's efficacy in addressing complex regression tasks for heat exchanger parameters. While the second layer leveraged the complementary strengths of CFNN and FN to achieve high accuracy, the third layer's refinement using CFNN as the optimal model further enhanced performance, delivering near-perfect predictive outcomes. These findings underscore the potential of the proposed hybrid DL framework to advance predictive modeling in engineering applications.

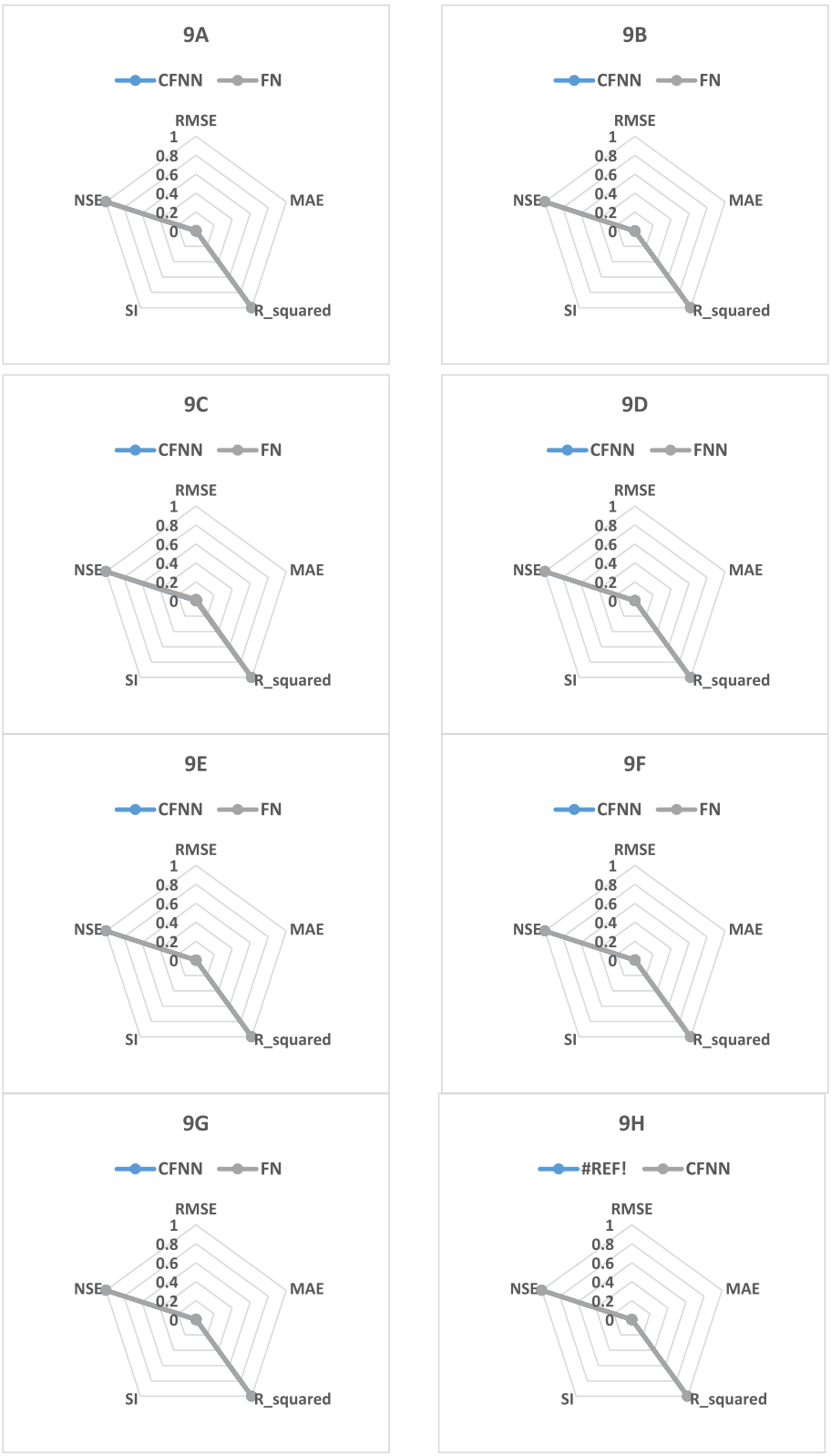

Fig. 9. Plots of metric evaluations for the second layer of the novel hybrid DL model. Figures with super indexes A, B, and C refer to the *Nu*, f, and P regression targets for the first dataset, respectively. Figures with super indexes D, E, and F refer to the *Nu*, f, and P regression targets for the second dataset, respectively. Figures with super indexes G, H, and I refer to three regression targets for the third dataset, respectively. Figures with super indexes J, K, and L refer to three regression targets for the fourth dataset, respectively. Figures with super indexes M, N, and O refer to three regression targets for the fifth dataset, respectively.

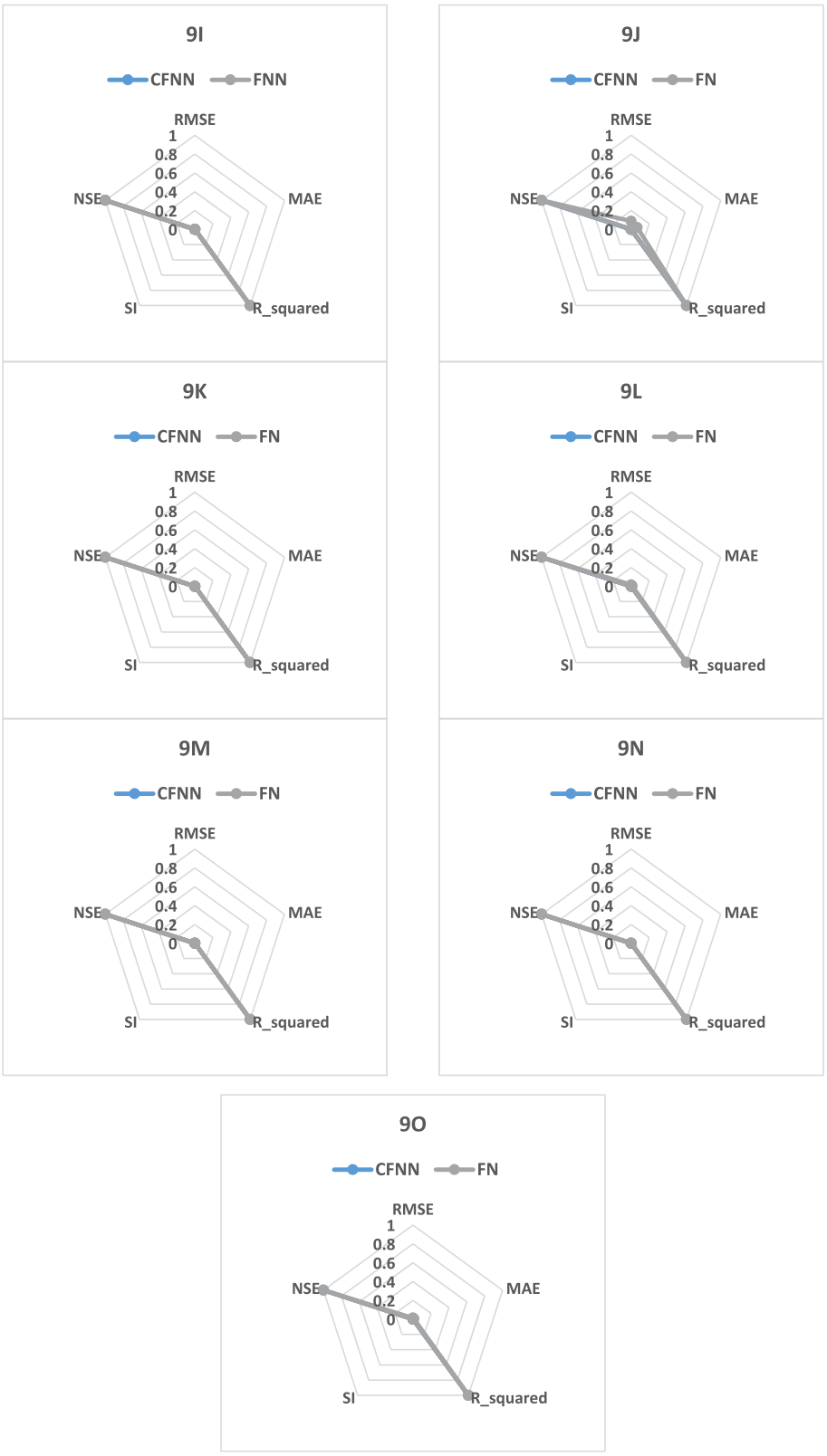

Fig. 9. (*continued*).

3.4. Performance comparison of traditional and hybrid DL models

3.4.1. Accuracy and prediction capabilities

The hybrid deep learning (DL) model exhibited superior predictive accuracy across all five datasets and scenarios when compared to the standalone performances of the traditional FN, CFNN, and FNN models. Also, the current work compared with the work in (Bakır et al., 2025). This improvement was particularly evident through reduced RMSE and MAE values, indicating enhanced accuracy and better generalization. For example, in Scenario 1, while FN produced an RMSE of 0.04, the

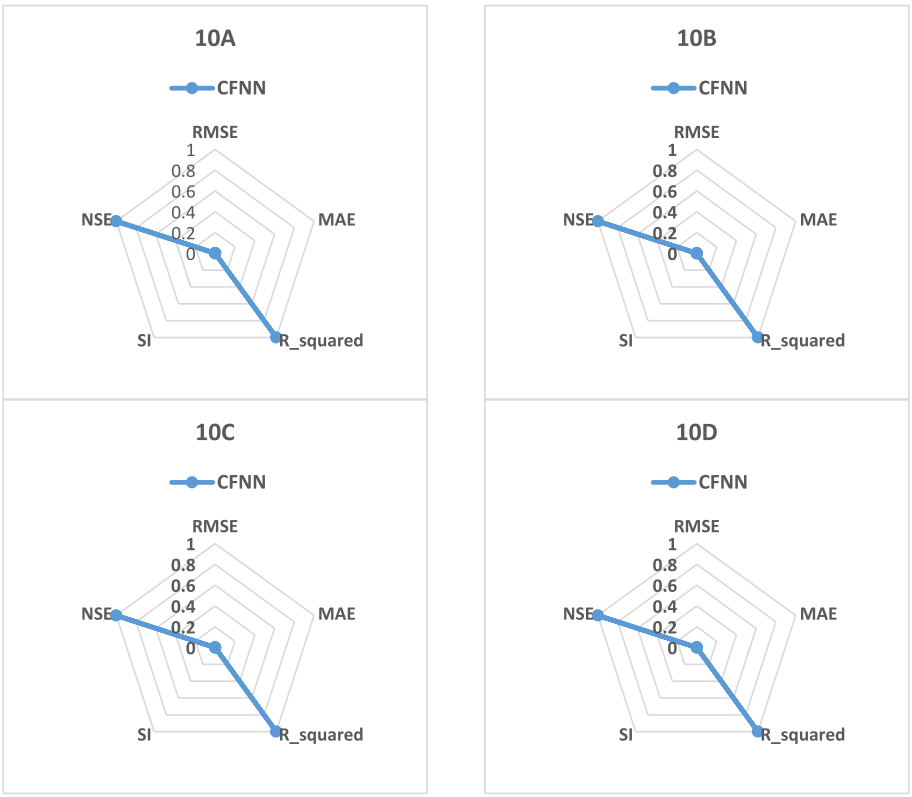

Fig. 10. Plots of metric evaluations for the third layer of the novel hybrid DL model. Figures with super indexes A, B, and C refer to the *Nu*, f, and P regression targets for the first dataset, respectively. Figures with super indexes D, E, and F refer to the *Nu*, f, and P regression targets for the second dataset, respectively. Figures with super indexes G, H, and I refer to three regression targets for the third dataset, respectively. Figures with super indexes J, K, and L refer to three regression targets for the fourth dataset, respectively. Figures with super indexes M, N, and O refer to three regression targets for the fifth dataset, respectively.

hybrid approach reduced this figure significantly to 0.005. Additionally, for Dataset 2, CFNN reported an MAE of 4.86 x 10^{-5}, whereas the hybrid model achieved a markedly lower value of 2.43 x 10^{-6}, demonstrating its superior predictive refinement. The findings suggest that the hybrid DL model enhances prediction accuracy by capitalizing on the advantages offered by its layered architecture.

3.4.2. *Robustness of predictions*

The hybrid DL model's multi-layer architecture demonstrated strong performance across various datasets and scenarios, consistently surpassing single-layer approaches. This was particularly evident from the higher R^2 values achieved for complex datasets, highlighting its superior ability to capture non-linear relationships. In Dataset 3, the FN model achieved an R^2 of 0.997, whereas the hybrid DL model improved this to 0.999, demonstrating a stronger correlation between predicted and actual values. The cascading framework effectively minimized prediction variance, making the hybrid DL model particularly advantageous for handling complex or noisy datasets.

3.4.3. *Computational efficiency*

Although the hybrid DL model features a multi-layer structure, it retained strong computational efficiency by selectively incorporating the top-performing models at each stage. This targeted refinement approach allowed the model to remain resource-efficient while maintaining high prediction accuracy.

4. Conclusion

This study introduces a novel hybrid deep learning (DL) model designed to predict key performance parameters of advanced plate heat exchanger APHE: Nusselt number (*Nu*), friction factor (f), and thermal performance parameter (P). The model integrates three DL methods—Feedforward Neural Network (FNN), Cascade Forward Neural Network (CFNN), and Fitting Network (FN)—in a systematic, multi-layered framework to optimize prediction accuracy and robustness. Evaluations conducted across five diverse datasets, each comprising three scenarios tailored to *Nu*, f, and P, highlight the efficacy of the proposed approach.

In the second layer of the hybrid model, CFNN and FN consistently emerged as the most effective DL models for most datasets and scenarios, achieving high predictive performance with R^2 values exceeding 0.9988 and RMSE values below 0.003. These models demonstrated their ability to minimize errors, especially in high-variability regions while preserving computational efficiency. The third layer, designed to refine the prediction further, identified CFNN as the optimal model for final predictions. This layer achieved near-perfect accuracy, with R^2 values surpassing 0.9999 and RMSE values as low as 2.4x10^{-6}, showcasing exceptional generalization and reliability.

The results demonstrate that the hybrid DL framework outperforms standalone DL models by leveraging their complementary strengths. The layered structure of the model ensures systematic feature refinement and iterative optimization at each stage, while the selection of best-performing models enhances computational efficiency and prediction accuracy. Furthermore, the adaptability of the hybrid approach makes it a promising tool for addressing complex regression tasks in engineering domains and beyond.

The key limitations of the proposed hybrid DL model are as follows:

1. **Computational Demands:** The multi-layer architecture requires higher computational resources compared to simpler models.

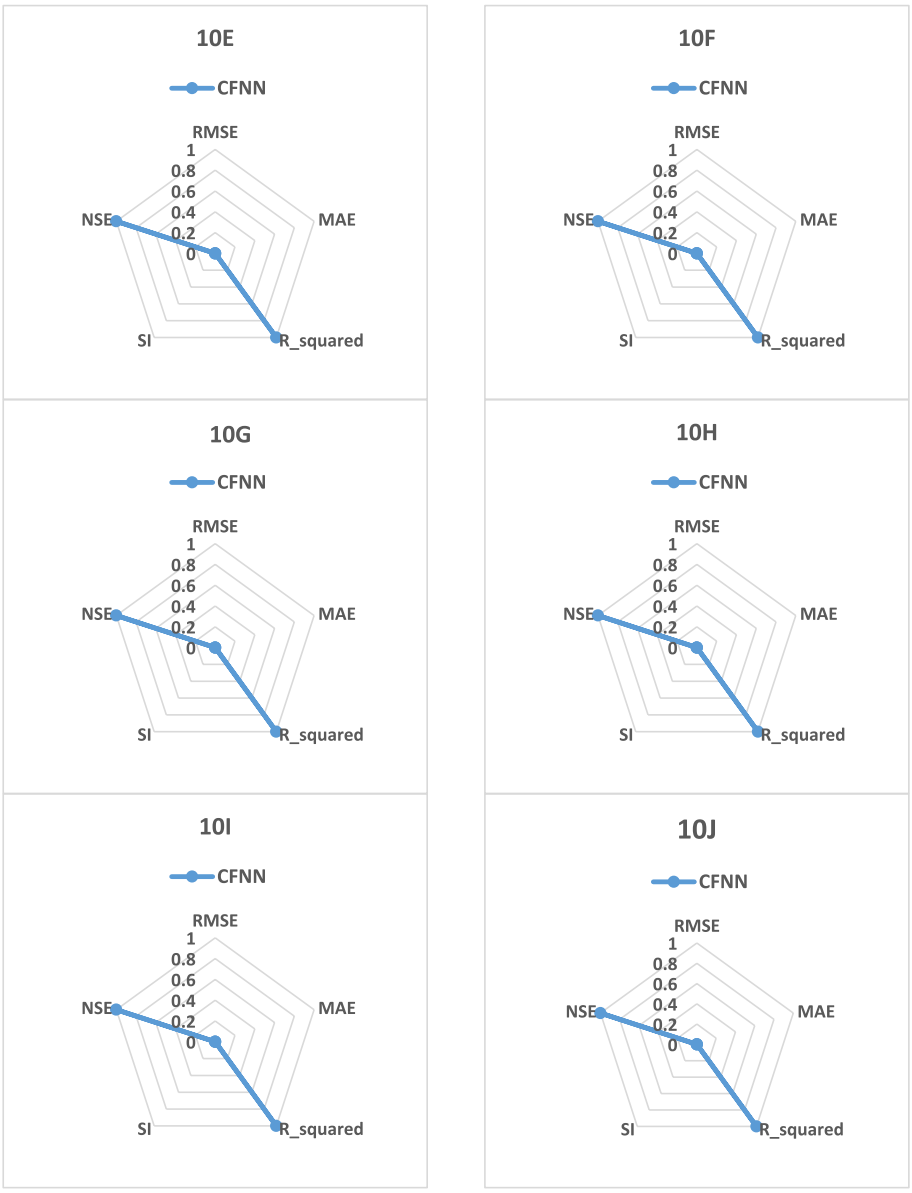

Fig. 10. (*continued*).

2. **Hyperparameter Selection:** Finding the optimal parameters for each layer is both time-intensive and complex.
3. **Overfitting Concerns:** Without additional regularization, the layered design may be prone to overfitting when applied to smaller datasets.

To address the identified limitations, the key future directions for the proposed hybrid DL model include:

1. **Enhancing Computational Efficiency:** Design lightweight frameworks and apply pruning strategies to lower computational costs without compromising accuracy.
2. **Automated Parameter Optimization:** Employ advanced techniques like Bayesian Optimization or Genetic Algorithms to streamline and improve hyperparameter selection.
3. **Real-Time Application and Scalability:** Modify the model for large-scale datasets and real-time use cases by cloud-based technologies and distributed computing systems.

CRediT authorship contribution statement

Ali A.H. Karah Bash: Writing – review & editing, Writing – original draft, Visualization, Software, Methodology, Formal analysis, Data curation. **Ahmad Aboul Khail:** Writing – original draft, Validation, Investigation, Conceptualization.

Availability of data and materials

We are still working on the dataset within the context of a project. The data that support the findings of this study are available upon reasonable request from the authors.

Funding

This research did not receive a specific grant from public, commercial, or not-for-profit funding agencies.

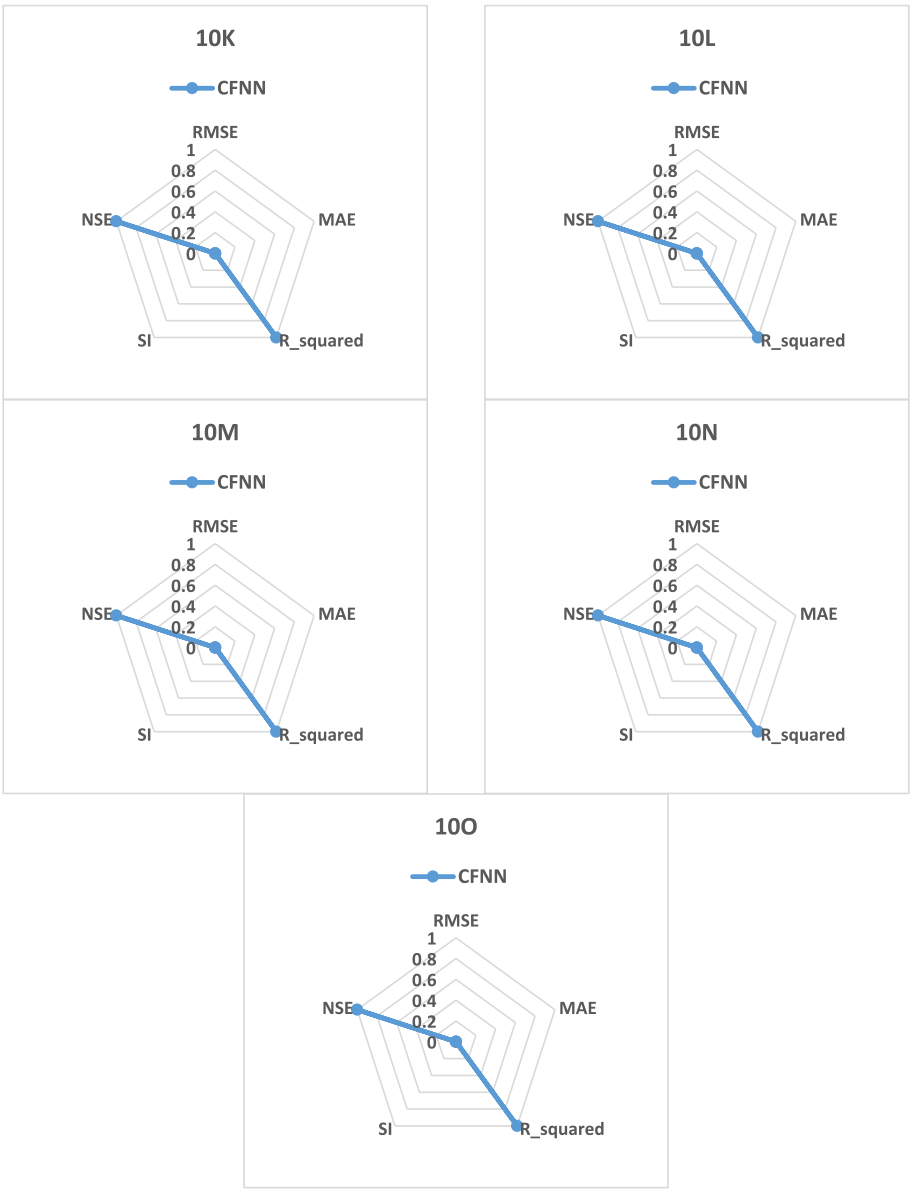

Fig. 10. (*continued*).

Declaration of competing interest

The authors declare that there are no known financial conflicts of interest or personal relationships that could have appeared to influence the work reported in this paper.

This research did not receive any specific grant from funding agencies in the public, commercial, or not-for-profit sectors.

All authors have approved the final version of the manuscript and agree to its submission to Engineering Applications of Artificial Intelligence.

Data availability

Data will be made available on request.

References

Aboul Khail, A., Erişen, A.J.T.S., Progress, E., 2022. Heat Transfer and Performance Enhancement Investigation of Novel Plate Heat Exchanger, vol. 34, 101368.

Aboul Khail, A., Erişen, A., 2021. Improvement of plate heat exchanger performance using a new plate geometry. Arabian Journal for Science Engineering 46 (3), 2877–2889.

Aboul Khail, A., Erişen, A., 2023. A review: CFD approaches of plate heat exchangers. Arch. Comput. Methods Eng. 30 (2), 1157–1165.

Aboul Khail, A., Bakır, R., Bakır, H., 2024. Prediction of thermo-hydraulic properties of flow in an innovative plate heat exchanger using machine learning algorithms. Physica Scripta 99 (10), 106004.

Amalfi, R.L., Kim, J., 2021. Machine learning-based prediction methods for flow boiling in plate heat exchangers. In: 2021 20th IEEE Intersociety Conference on Thermal and Thermomechanical Phenomena in Electronic Systems (iTherm). IEEE.

Bakır, R., Aboul Khail, A., Bakır, H., 2025. Enhancing the prediction of flow characteristics in an inventive plate heat exchanger using deep learning techniques. Physica Scripta 100 (3), 035114.

Ebbs-Picken, T., et al., 2024. Deep Encoder–Decoder Hierarchical Convolutional Neural Networks for Conjugate Heat Transfer Surrogate Modeling, vol. 372, 123723.

Godasiaei, S.H., Chamkha, A.J., 2024a. Numerical Heat Transfer,Part A: Applications, *Exploring Novel Heat Transfer Correlations: Machine Learning Insights for Molten Salt Heat Exchangers*, pp. 1–18.

Godasiaei, S.H., Chamkha, A.J., 2024b. Numerical heat transfer,part A: Applications, *Exploring The Influence of Crystallization Fouling on Microscale Heat Exchangers through Machine Learning Analysis*, pp. 1–27.

Guo, Z., et al., 2024. Constraint-incorporated Deep Learning Model for Predicting Heat Transfer in Porous Media under Diverse External Heat Fluxes, vol. 18, 100425.

Hong, D., et al., 2023. Cross-city Matters: A Multimodal Remote Sensing Benchmark Dataset for Cross-City Semantic Segmentation Using High-Resolution Domain Adaptation Networks, vol. 299, 113856.
Hong, D., et al., 2024. SpectralGPT: Spectral Remote Sensing Foundation Model.
Hosseini, S., et al., 2022. Novel and Robust Machine Learning Approach for Estimating the Fouling Factor in Heat Exchangers, vol. 8, pp. 8767–8776.
Jilak, A., Assareh, E., Nedaei, M., 2017. Application of a novel multi-objective optimisation method integrated with the artificial neural networks for optimum design of a plate heat exchanger. Aust. J. Mech. Eng.
Jilak, A., Assareh, E., Nedaei, M., 2020. Application of a Novel Multi-Objective Optimisation Method Integrated with the Artificial Neural Networks for Optimum Design of a Plate Heat Exchanger. Australian Journal of Mechanical Engineering.
Jin, B., 2024. X.J.A.J.o.E. Xu, and Banking, Wholesale Price Forecasts of Green Grams Using the Neural Network (ahead-of-print).
Jin, B., Xu, X.J.I., Steelmaking, 2024a. Machine Learning Predictions of Regional Steel Price Indices for East China, 03019233241254891.
Jin, B., Xu, X., 2024b. Pre-owned housing price index forecasts using Gaussian process regressions. Journal of Modelling in Management 19 (6), 1927–1958.
Jin, B., Xu, X.J.A.S., 2024c. Carbon emission allowance price forecasting for China Guangdong carbon emission exchange via the neural network. Global Finance Review 6 (1), 3491, 2016. pp. 2593–2620.
Kakac, S., et al., 2012. Condensers and Evaporators, pp. 355–400.
Khan, J.S., et al., 2023. Artificial intelligence based prediction of optimum operating conditions of a plate and fin heat exchanger under uncertainty: a gray-box approach. Int. J. Heat Mass Tran. 217, 124653.
Li, Y., Chang, J.J.A.S., 2023. Technology. Research on time sequence prediction of supersonic cascade flow field based on compressed sensing artificial neural network 142, 108684.
Longo, G.A., et al., 2020. Machine Learning Approach for Predicting Refrigerant Two-phase Pressure Drop inside Brazed Plate Heat Exchangers (BPHE), vol. 163, 120450.
Mudhsh, M., et al., 2023. Modelling of thermo-hydraulic behavior of a helical heat exchanger using machine learning model and fire hawk optimizer. Case Stud. Therm. Eng. 49, 103294.
Peng, H., Ling, X., 2008. Optimal design approach for the plate-fin heat exchangers using neural networks cooperated with genetic algorithms. Appl. Therm. Eng. 28 (5–6), 642–650.
Peng, H., Ling, X., 2009. Neural networks analysis of thermal characteristics on plate-fin heat exchangers with limited experimental data. Appl. Therm. Eng. 29 (11–12), 2251–2256.
Saeed, M., et al., 2022. Performance Enhancement of a C-Shaped Printed Circuit Heat Exchanger in Supercritical CO2 Brayton Cycle: A Machine Learning-Based Optimization Study, vol. 38, 102276.
Sammil, S., Sridharan, M., 2024. Employing ensemble machine learning techniques for predicting the thermohydraulic performance of double pipe heat exchanger with and without turbulators. Therm. Sci. Eng. Prog. 47, 102337.
Seawram, S., et al., 2022. Specific Heat Capacity Prediction of Hybrid Nanofluid Using Artificial Neural Network and its Heat Transfer Application, vol. 8, pp. 8–15.
Shah, Z., et al., 2024. Multilayer deep-learning intelligent computing for the numerical analysis of unsteady heat and mass transfer in MHD Carreau Nanofluid model, 64, 105369.
Uguz, S., Ipek, O., 2022a. Prediction of the parameters affecting the performance of compact heat exchangers with an innovative design using machine learning techniques. J. Intell. Manuf. 33 (5), 1393–1417.
Uguz, S., Ipek, O., 2022b. Prediction of the parameters affecting the performance of compact heat exchangers with an innovative design using machine learning techniques. Journal of Intelligent Manufacturing 33 (5), 1393–1417.
Wang, Q., et al., 2021. Bubble Recognizing and Tracking in a Plate Heat Exchanger by Using Image Processing and Convolutional Neural Network, vol. 138, 103593.
Wang, Y., et al., 2025. A Data-Driven Model for Steel Bridge Temperature Behaviour Based on Deep Learning Technology and Heat Transfer Analysis, vol. 322, 119084.
Wen, S., et al., 2025. Numerical Simulation Investigation of Heat Exchangers for Active Chilled Beams Based on Neural Networks and a Genetic Algorithm, vol. 378, 124818.
Wu, X., et al., 2021. Convolutional neural networks for multimodal remote sensing data classification, 60, 1–10.

Update

Engineering Applications of Artificial Intelligence

Volume 152, Issue , 15 July 2025, Page

DOI: https://doi.org/10.1016/j.engappai.2025.110869

Engineering Applications of Artificial Intelligence 152 (2025) 110869

Contents lists available at ScienceDirect

Engineering Applications of Artificial Intelligence

journal homepage: www.elsevier.com/locate/engappai

Corrigendum

Corrigendum to "Advanced multi-layer deep learning model for accurate estimation of heat transfer and flow designing parameters across diverse dataset configurations" [Eng. Appl. Artif. Intell. 151 (2025) 110723]

Ali A.H. Karah Bash [a], Ahmad Aboul Khail [b,*]

[a] Department of Electrical and Electronic Engineering, Faculty of Engineering, Hasan Kalyoncu University, Şahinbey, 27110, Gaziantep, Türkiye
[b] Department of Mechanical Engineering, Faculty of Engineering, Hasan Kalyoncu University, Şahinbey, 27110, Gaziantep, Türkiye

The authors regret that affiliation "c" was inadvertently included in the article due to an oversight during the manuscript preparation. They kindly request the removal of affiliation "c" from the published article.

The authors would like to apologise for any inconvenience caused.

DOI of original article: https://doi.org/10.1016/j.engappai.2025.110723.
* Corresponding author.
E-mail addresses: khailnuc@gmail.com, ahmed.sadik@hku.edu.tr (A.A. Khail).

https://doi.org/10.1016/j.engappai.2025.110869

Available online 15 April 2025